Chemie der Erde 77 (2017) 596–613

Contents lists available at ScienceDirect

Chemie der Erde

journal homepage: www.elsevier.com/locate/chemer

Geochemistry of black shales from the Mesoproterozoic Srisailam Formation, Cuddapah basin, India: Implications for provenance, palaeoweathering, tectonics, and timing of Columbia breakup

Himadri Basu[a,*], P.S. Dandele[b], K. Ramesh Kumar[a], K.K. Achar[a], K. Umamaheswar[a]

[a] Atomic Minerals Directorate for Exploration and Research, 1-10-153-156, S.P. Road, Begumpet, Hyderabad 500 016, India
[b] Regional Centre for Exploration and Research, AMD/CR, Civil Lines, Nagpur 440 001, India

ARTICLE INFO

Keywords:
Black shale
Palaeoweathering
Tectonics
Srisailam Formation
Cuddapah basin
India
Columbia

ABSTRACT

The Mesoproterozoic Srisailam Formation, exposed along the northern part of the Cuddapah basin, India, comprises mainly medium- to fine-grained siliciclastics, and is devoid of any carbonate sediment. Preliminary sedimentological studies helped in recognizing fifteen distinct facies (five facies associations) in Chitrial outlier of the Srisailam Formation deposited in continental half-graben basin(s). Black shales (*sensu lato*) are minor components of the Srisailam Formation, and inferred to have deposited in deep lacustrine and prodelta facies of the half-graben(s). The black shales show restricted thickness (up to 29.0 m), and are characterized by overall high 'black shale' to 'total shale' ratio (> 0.51). Their geochemical characteristics were studied to constrain provenance, palaeoclimate, and tectonic setting of deposition of the Srisailam Formation. Further, an attempt has been made to use the Srisailam black shales as proxy for constraining the timing of breakup of the supercontinent Columbia.

The Srisailam black shales are geochemically quite distinct. At similar SiO_2 contents they are considerably different from PAAS. They are characterized by considerably lower ΣREE (Av. 136.0 ± 50.4 ppm) but a more conspicuous negative Eu-anomaly (Av. 0.34 ± 0.09) than PAAS. Al_2O_3/TiO_2 and TiO_2/Zr ratios coupled with Eu/Eu*, Gd_{CN}/Yb_{CN}, La/Sc, Th/Sc, and Th/Cr ratios suggest their derivation from granite and granodiorite. The CIA values (65–90, Av. 72 ± 9) as a whole indicate moderate chemical weathering under semiarid climate. Discriminating geochemical parameters indicate passive margin depositional setting. The combined sedimentological and geochemical characteristics reveal deposition of the Srisailam sediments in continental rift basin(s).

Thick succession of black shales (with high CIA values) that deposited with shelf carbonates proxy for mantle superplume and supercontinent breakup events. The sedimentological characteristics and geochemical data of the Srisailam black shales plausibly exclude any large-scale breakup of Columbia during the interval (1400–1327 Ma) of deposition of the Srisailam Formation.

1. Introduction

The geochemistry of mudrocks is commonly used as sensitive indicator of provenance character (Cullers, 2000), palaeoclimate and palaeoweathering conditions (Nesbitt and Young, 1982; Fedo et al., 1995), and tectonic settings of sedimentary basins (Roser and Korsch, 1986; McLennan et al., 1990). It is also used to evaluate the composition, and understand the evolution of the continental crust (Taylor and McLennan, 1985; Condie, 1993). Being fine grained and impermeable, mudrocks preserve the near-original geochemical signature of the provenance composition (Paikaray et al., 2008 and references therein). Mudrocks provide more information about the regional tectonic settings than the associated sandstones (Cullers and Podkovyrov, 2000). Though, most mudrocks are formed in restricted basin environments in specific tectonic settings (Cox and Lowe 1995), black shale, a dark-coloured mudrock (Swanson, 1961), is found in a wide spectrum of geological settings over the entire span of the geological time (Tourtelot, 1979). Nevertheless, the deposition of the Precambrian black shales has been considered by several researchers to be more important in some tectonic settings (Condie et al., 2001). Such 'tectonic bias' often puts constraints in understanding the evolution of especially the Precambrian black shales in a specific geological setting. Under

* Corresponding author.
E-mail addresses: himadri.amd@gmail.com (H. Basu), psdandele.amd@gov.in (P.S. Dandele), krameshkumar.amd@gov.in (K.R. Kumar), kiranachar1953@gmail.com (K.K. Achar), umamaheswark252@gmail.com (K. Umamaheswar).

http://dx.doi.org/10.1016/j.chemer.2017.10.002
Received 12 January 2017; Received in revised form 29 June 2017; Accepted 6 October 2017

such circumstances geochemical characteristics of black shales may be of immense use in understanding their provenance, weathering conditions, and depositional settings. Further, a global correlation between the deposition of especially the Proterozoic black shales and mantle superplume as well as supercontinent formation/breakup events has been observed (Condie et al., 2001; Condie, 2004). The thickness and CIA (Chemical Index of Alteration; Nesbitt and Young, 1982) of black shales, deposited in passive margin, intracratonic, or platformal basins, could be used as proxies for mantle superplume and supercontinent formation/breakup events (Condie et al., 2001; Condie, 2004).

Black shales have been reported from the Neoarchaean Sandur greenstone belt (Manikyamba and Kerrich, 2006), and a number of Proterozoic intracratonic basins in Peninsular India (Murty et al., 1962; Pandalai et al., 1983; Banerjee et al., 2006; Manikyamba et al., 2008) as well as from the extra-peninsular Himalayan belt (Rawat et al., 2010; Williams et al., 2012). In spite of availability of huge volume of black shales in the Proterozoic Cuddapah basin, there is a dearth of studies on their geochemical aspects for understanding the provenance and its compositional variation with time, tectonic evolution of different subbasins of the Cuddapah basin, and the realm of palaeoclimatic conditions under which weathering and erosion of provenance took place. Only Manikyamba et al. (2008) studied the geochemical characteristics of the black shales of the Cumbum Formation for tracing provenance and tectonic setting of the basin, and evaluating weathering intensity of the provenance. In order to bridge this gap, the present study is focused on understanding the provenance of the Mesoproterozoic Srisailam Formation, its palaeoweathering, and tectonic evolution of the Srisailam subbasin in the northern part of the Cuddapah basin (Fig. 1a) from mainly the geochemical characteristics of the Srisailam black shales. Preliminary sedimentological studies have also been carried out for better understanding of the geochemical signatures and making the geochemical interpretations especially on tectonic evolution more meaningful. The Srisailam black shales have also been used as potential proxy to constrain the timing of breakup of the supercontinent Columbia that has long been debated.

2. Geological setting

The Proterozoic Cuddapah basin is located in the central part of the Eastern Dharwar Craton, India (Fig. 1a). It is a polyphase basin, and sedimentation in this basin took place in a series of successively evolved, spatially distributed but interconnected subbasins viz. Papaghni, Nallamalai, Srisailam, and Kurnool-Palnad (Fig. 1a; Basu et al., 2014 and references therein). The sediments of the Cuddapah basin range in age from Palaeoproterozoic to Neoproterozoic (Fig. 1b), and the Mesoproterozoic Srisailam Formation was deposited in the Srisailam subbasin located in the northern part of the Cuddapah basin (Fig. 1a). The Neoarchaean gneisses (Pb–Pb age of 2638 ± 94 Ma; Vimal et al., 2012), thin slivers of greenstone belt (Peddavoora schist belt), Palaeoproterozoic granitoids (Pb–Pb age of 2442 ± 13 Ma; Pandey et al., 2009), and mainly WNW-ESE/NW-SE, N-S/NNE-SSW to minor NE-SW trending Palaeoproterozoic (Sm-Nd age of 2173 ± 64 Ma; Pandey et al., 1997) gabbro/dolerite dykes, N-S/NNE-SSW to NE-SW trending quartz reefs form the basement for the Srisailam sediments to the north (Fig. 1a and c). In contrast, the sediments of the late Palaeoproterozoic to early Mesoproterozoic (1659 ± 22 Ma to ~1590 Ma) Nallamalai Group (Saha, 2002; Collins et al., 2015) form the basement to the south (Fig. 1a and c). The Srisailam Formation comprises mainly quartzite (sandstone), siltstone, shale (Nagaraja Rao et al., 1987; Lakshminarayana et al., 2001), and is characteristically devoid of any carbonate sediment. The Srisailam Formation is approximately 620 m thick at Srisailam type area (Murthy, 1979). However, recent borehole data revealed a maximum thickness of 419 m at Kottapullareddipuram (Fig. 1c; Banerjee et al., 2012). The sedimentary succession of the Srisailam Formation has variously been interpreted to be the deposits of shallow marine/tidal flat (Nagaraja Rao et al., 1987), shoreline to intertidal sand flat environments with fluvial influence (Lakshminarayana et al., 2001). However, a detailed analysis of facies and sedimentological study is not available till date. The sediments of the Srisailam Formation have been affected by mainly E–W to NW-SE trending faults and N-S/NNE-SSW trending lineaments/fractures. The sediments are generally unmetamorphosed. A horse-shoe shaped outlier (~60 sq km) of the Srisailam Formation, occurring near Chitrial village, Nalgonda district, India (hereafter Chitrial outlier; Fig. 1c), along the northern periphery of the Srisailam subbasin (Fig. 1a and c) represents the geological domain for this study.

In Chitrial outlier, the Srisailam Formation occurs as flat-lying to gently (5–8°) SE-dipping strata. It comprises variably sorted arenaceous siliciclastics, subordinate argillaceous and minor rudaceous sediments. The sediments have been affected by post-sedimentary faults. Locally, mild warping has also been observed in the sediments. Dominantly coarse-grained to often porphyritic, grey biotite-granite to locally leucogranite form the basement for the Srisailam sediments in Chitrial outlier. Neoarchaean tonalite-granodiorite-adamellite (TGA) suite of rocks has been reported (Vimal et al., 2012) from the vast terrane occurring farther east and northeast of the study area, especially east and northeast of NW-SE trending Peddavoora schist belt (Fig. 1a and c).

3. Age constraints and palaeolatitude

3.1. Stratigraphic correlation

The stratigraphic correlation of the Srisailam Formation has long been debated. The lithostratigraphic correlation established by King (1872) was exclusively followed for almost a century. King (1872) considered the Srisailam sediments (Sreeshalum Quartzites) to be the youngest member of the 'Kistnah Group' (now non-existent nomenclature; Table S1) that comprises successively older Kolamnala (Kolumnullah) Slates and Irlakonda (Irlaconda) Quartzites, and overlies the Cumbum Slates and Bairenkonda (Byrenconda) Quartzites of the Nallamalai (Nullamullay) Group with a doubtful unconformity. However, Rajurkar and Ramalingaswami (1975) were first to differ, and consider the Srisailam Quartzite (Formation) as the youngest member of the Cumbum Slate (Formation). They omitted the Kistnah Group (Table S1), and opined that all its constituent members are parts of the Cumbum Slate. The Irlakonda Quartzite was shown to be lateral lithofacies variation of the Cumbum Slate (Nagaraja Rao et al., 1987). In contrast, Meijerink et al. (1984) considered the Srisailam sediments to be the youngest formation of the Bairenkonda (Quartzite) Subgroup (Fig. 1b; Table S1). Subsequently Nagaraja Rao et al. (1987), on the basis of identification of unconformable relationship with the Kolamnala Shale (equivalent to the Cumbum Shale) at a number of places, established the Srisailam Formation to be younger than the Nallamalai Group (Fig. 1b), and accepted the nomenclature 'Kistnah Group' as redundant. Their stratigraphic positioning of the Srisailam Quartzite was similar to that proposed by Dutt (1975). Saha (2002) also reported the Srisailam Formation to unconformably overlie the Cumbum Formation of the Nallamalai Group. In the light of this latest well-accepted lithostratigraphic correlation, the regional litho-structural relationship and igneous intrusive events have been considered here to bracket the age of the Srisailam Formation.

3.2. Age constraints

The sediments of the late Palaeoproterozoic to early Mesoproterozoic (1659 ± 22 Ma to ~1590 Ma) Nallamalai Group (Saha, 2002; Collins et al., 2015), underlying the Srisailam Formation, have been intruded by the Vellaturu Granite (Fig. 1a) at ~1575 Ma (Crawford and Compston, 1973). Further, Racherla syenite and Chelima lamproite ($^{40}Ar/^{39}Ar$ age of 1417.8 ± 8.2 Ma; Chalapathi Rao et al., 1999) intrude the sediments of the Nallamalai Group (Fig. 1a). A number of coeval lamproites have been reported also from the

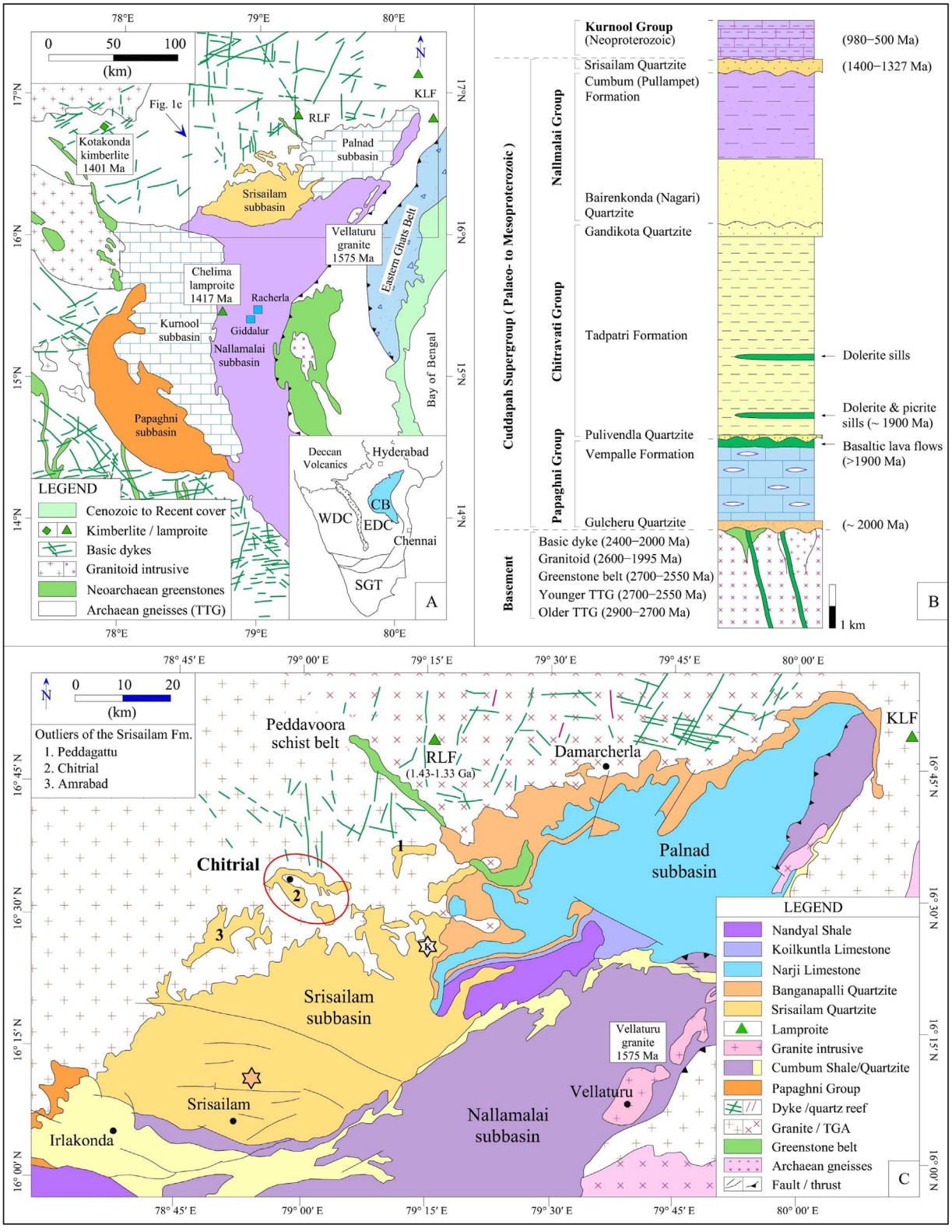

Fig. 1. (A) Geological map of the southern Indian Peninsula showing location of the Cuddapah basin (inset) and spatial distribution of its different subbasins. WDC, Western Dharwar Craton; EDC, Eastern Dharwar Craton; SGT, Southern Granulite Terrane; CB, Cuddapah basin; RLF, Ramadugu lamproite field; KLF, Krishna lamproite field. Geology of the EDC is after French et al. (2008) and references therein; (B) Generalized lithostratigraphic succession of the Cuddapah basin (after Nagaraja Rao et al., 1987; Basu et al., 2014). The age of the Srisailam Formation is constrained at ~1400–1327 Ma (see text for details); (C) Geological map of the northern part of the Cuddapah basin (modified after Krishnaswamy et al., 1981) showing the location of Chitrial outlier. Open star, location of aeolian sediments reported (Biswas, 2005) from the Srisailam subbasin; Open star with letter 'K', location of maximum thickness of the Srisailam Formation intercepted in borehole (Banerjee et al., 2012). TTG, tonalite-trondhjemite-granodiorite; TGA, tonalite-granodiorite-adamellite. The study area is marked with an ellipse. Solid circles are important localities.

Table 1
Details of different facies identified in the Srisailam Formation, Srisailam subbasin.

Facies association	Facies name	Facies characteristics	Remarks
Facies Association I (FA-I): Alluvial fan/fan-delta association	Facies A: Proximal fan conglomerate to pebbly sandstone	Pebble-conglomerate to coarse-grained pebbly sandstone; unsorted and ungraded to often normally graded, some clasts are near-vertical; dominantly subangular to subrounded quartz and minor feldspar clasts; dominantly sandy matrix with often subordinate silt and mud; conglomerate is clast-supported to sandy matrix-supported.	Facies A passes upward through Facies B to Facies C, and all of them thin-out towards basin interior. Sediments of this facies association generally occur at the base of the sedimentary succession. However, they are often found interlayered with the sediments of other facies as well.
	Facies B: Mid-fan fine-pebble-conglomerate to coarse-grained sandstone (Fig. 3a)	Ungraded, unsorted fine-pebble-conglomerate passing upward into coarse-grained, grey to dull-greenish-grey sandstone, often outsized pebbles float in the middle of the facies; dominantly subangular to subrounded quartz and minor feldspar clasts; dominantly fine-grained sandy matrix with often subordinate silt and mud.	
	Facies C: Distal fan granule-conglomerate and sandstone couplets (Fig. 3b)	Stacked, thin (3–11 cm) depositional couplets (grey to dull-greenish-grey) of granule-conglomerate to coarse-grained sandstone and medium- to fine-grained sandstone; erosive bases; locally sands and granules are planar cross-stratified; occasionally contains paper-thin dark-grey shale laminations conforming to the micro-relief produced by the coarser sediments.	
Facies Association II (FA-II): Delta top association	Facies E: Delta channel (distributary channel) sandstone	Coarse- to medium-grained unsorted sandstone grading upward to thinly bedded to thickly laminated fine-grained sandstone or siltstone; sandstone is often granular in the lower part of the facies; frequently 10–15 cm thick fine-pebble-conglomerate occurs at the base; sandstone is feldspathic to sub-feldspathic, massive to cross-stratified, lower contact sharp/erosional, upper contact gradational with delta plain mudrock.	Distinction between facies K_1 and N could not often be done in cores, and they presumably coalesce with each other to form thin sheet-like body of laminated siltstone and shale.
	Facies K_1: Delta plain mudrock	Intercalation of plane-laminated siltstone (1–3 mm) and grey shale (< 1 mm), convolute laminations at places; gradational lower contact with underlying delta channel sandstone but sharp upper contact with crevasse splay sandstone.	
	Facies H: Crevasse splay sandstone	Medium- to often coarse-grained grey sandstone; variation in grain-size and minor mud drapes or shale streaks define bedding; gradational upper and sharp lower contacts with delta plain mudrock; 7–10 cm thick but may be up to 40 cm.	
	Facies N: Interdistributary bay mudrock	Intercalation of millimetre-scale grey to dark-grey siltstone and shale; wavy and lenticular bedding; gradational lower contact with underlying mouthbar sandstone (Fig. 3c) but sharp upper contact with delta channel sandstone.	
Facies Association III (FA-III): Delta front association	Facies D: Mouthbar sandstone	Fine- to dominantly medium-grained, unsorted sandstone with thin (5–7 cm), coarse-grained sandstone or granule-conglomerate at the base; overall grain-size decreases upward; sandstone is feldspathic to sub-feldspathic, massive to cross-stratified; often randomly oriented ripped-up grey shale chips or plates occur in sandy part; sharp and erosional lower contact; up in the facies fine-grained sandstone grades to laminated siltstone-shale of interdistributary bay or delta plain.	
	Facies I: Delta slope siltstone to fine sandstone (Fig. 3d)	Dominantly fine-grained sandstone to siltstone with subordinate medium- and minor coarse-grained sandstone, and grey/dark-grey shale; sand fraction increases upward; abundant synsedimentary deformation features like convolute laminations, slump structures, small faults; locally abundant randomly oriented grey shale plates and streaks occur in sandy upper part.	
	Facies J: Prodelta siltstone-shale (Fig. 3e)	Thin, horizontally laminated, grey to dark-grey siltstone and shale grading to dark-grey/black shale; up in the facies siltstone to very fine-grained sandstone intercalations become more conspicuous; siltstone laminae are planar to gently wavy, laterally discontinuous with diffused upper and lower contacts; frequent millimetre-scale load and flame structures; interfingering upper contact with delta slope sediments, and grades down-dip into deep lacustrine deposits; abundant disseminated pyrite.	

(*continued on next page*)

Table 1 (*continued*)

Facies association	Facies name	Facies characteristics	Remarks
Facies Association IV (FA-IV): Lacustrine association	Facies F: Near-shore lacustrine sandstone	Fine- to medium-grained, massive to cross-stratified sandstone passing upward to thinly bedded, fine-grained sandstone or siltstone; feldspathic to sub-feldspathic in composition; planar-tabular cross-stratification, wave ripples are frequent; rare hummocky cross-stratification; laterally persistent over several tens of kilometres.	The sediments of this facies association extend over considerable distances.
	Facies L: Shallow lacustrine laminated silty-sandstone	Thickly laminated to thinly bedded, plane parallel fine-grained sandstone to siltstone; minor wavy bedding, locally thin shale lamination with load and flame structures; laterally persistent over hundreds of metres to several kilometres.	
	Facies M: Deep lacustrine laminated shale (Fig. 3f)	Thin, horizontally laminated dark-grey/black shale with intercalation of thinly laminated grey to dark-grey siltstone and minor fine-grained muddy sandstone; occasional convolute laminations; abundant pyrite.	
Facies Association V (FA-V): Fluvial association	Facies G: Channel sandstone (Fig. S2)	Light-pinkish-brown to grey, fine- to medium-grained sandstone with subordinate coarser sandstone, and minor granule- and fine-pebble-conglomerate; sandstone is feldspathic to sub-feldspathic, planar and trough cross-stratified, locally massive; sometimes foreset laminae of large-scale planar-tabular cross-stratification show normal grading; gently concave-up erosional lower bounding surfaces; sheet-like body and laterally persistent over several tens of kilometres.	The laterally amalgamated channel sands occur as sheet-like body. Often the channel sands show evidence of aeolian reworking (Fig. S3).
	Facies K_2: Fluvial overbank sediments	Intercalation of plane-laminated millimetre-scale creamy-yellow to light-purple shale/claystone with interlayering of lenses or laminae of silt or fine-grained sandstone; sand laminae are up to 6 mm thick; thin sheet-like body; lower contact gradational with channel sandstone.	

basement to the northern/northwestern outskirt (e.g. Ramadugu lamproite field; Chalapathi Rao et al., 2014) of the Srisailam subbasin. However, as on date nowhere these igneous bodies have been reported to intrude the sediments of the Srisailam Formation. It has been suggested that the emplacement of syenite (Racherla; Fig. 1a), and lamproite (Chelima; Fig. 1a) in this part of the Eastern Dharwar Craton led to the formation of the Srisailam subbasin through localized crustal heating, domal upwarping, and subsequent gravity induced block faulting (Chatterjee and Bhattacharji, 2001). Therefore, the maximum age of the Srisailam Formation may reasonably be put at ~1400 Ma.

The Srisailam Formation has not been intruded by any igneous body. Therefore, its minimum age has been inferred from the age of the associated epigenetic uranium mineralization. Uranium mineralization associated with the Mesoproterozoic unconformity between the Srisailam Formation and the basement granite has been reported from Chitrial and surrounding outliers (Parihar and Rao, 2012). Pandey et al. (2009) obtained a Sm-Nd isochron age of 1327 ± 170 Ma with an initial εNd value of −12.0 ± 2.3 on uraninite grains separated from mineralized samples of the Srisailam Formation. The Pb-isotope ratio ($^{208}Pb/^{204}Pb$) in galena from the mineralized zone was found to be similar to that of unleached uraninite grains. On the basis of these data an initial stage of uranium mineralization in the Srisailam Formation has been suggested at ~1300 Ma (Pandey et al., 2009). These suggest that the minimum age of the Srisailam Formation may approximately be set at 1327 Ma, and the age of the Srisailam Formation may be bracketed between 1400 and 1327 Ma. However, precise isotopic age constraints are still awaited for the Srisailam Formation.

3.3. Palaeolatitue

The Mesoproterozoic global palaeogeographic reconstruction, based on palaeomagnetic data, indicates mid-latitude positions of a major part of the Indian subcontinent, especially the Cuddapah basin (Figs. 13–15 in Pisarevsky et al., 2014), during 1450–1270 Ma. Palaeomagnetic data of ~1.2 Ga Harohalli dykes of the Dharwar craton places India at polar latitudes (Pradhan et al., 2009). Therefore, the palaeomagnetic data indicate mid-latitude position of the Cuddapah basin during the time-frame of deposition of the Srisailam Formation.

4. Sedimentary facies and depositional environments

The sedimentological features of the Srisailam Formation were studied to understand the depositional environment and basinal tectonics, and therefore, to aid the interpretation of geochemical signatures. The sedimentological characteristics of different facies are rarely observable in surface exposures due to the occurrence of light-brownish-pink to grey sandstone capping all other lithologies. Similarly, rubble-covered or escarped nature mostly prevented any detailed sedimentological study along the margin of the outlier(s). Therefore, emphasis was given on the study of drill-cores for understanding the vertico-lateral lithological variations and facies identification.

The Srisailam Formation in Chitrial outlier dominantly comprises light-brownish-pink to grey sandstone (feldspathic/sub-feldspathic arenite), light-purple or dull-greenish-grey shale, light- to dark-grey siltstone frequently intercalated with shale (shaly-siltstone to silty-shale), light-grey to dark-grey/black shale (Fig. S1), dull-greenish-grey to grey quartzose sandstone (quartz arenite), and granular to fine-pebble-conglomerate. The thickness of the sediments reaches up to a maximum of 133 m (borehole data). Dark-grey/black shales are common towards the base, and often in the lower-middle part of the sedimentary succession. However, massive varieties (mudstones) have also been observed rarely. Thicknesses of different shale and silty-shale units, as observed in drill-cores of any particular borehole, were measured and added to obtain the 'total shale' thickness at that location (section). Similarly, the thicknesses of all grey to dark-grey/black shale and silty-shale units in the same borehole were added to obtain 'black shale' thickness at that location. Thin (< 5 cm) intercalations of fine-

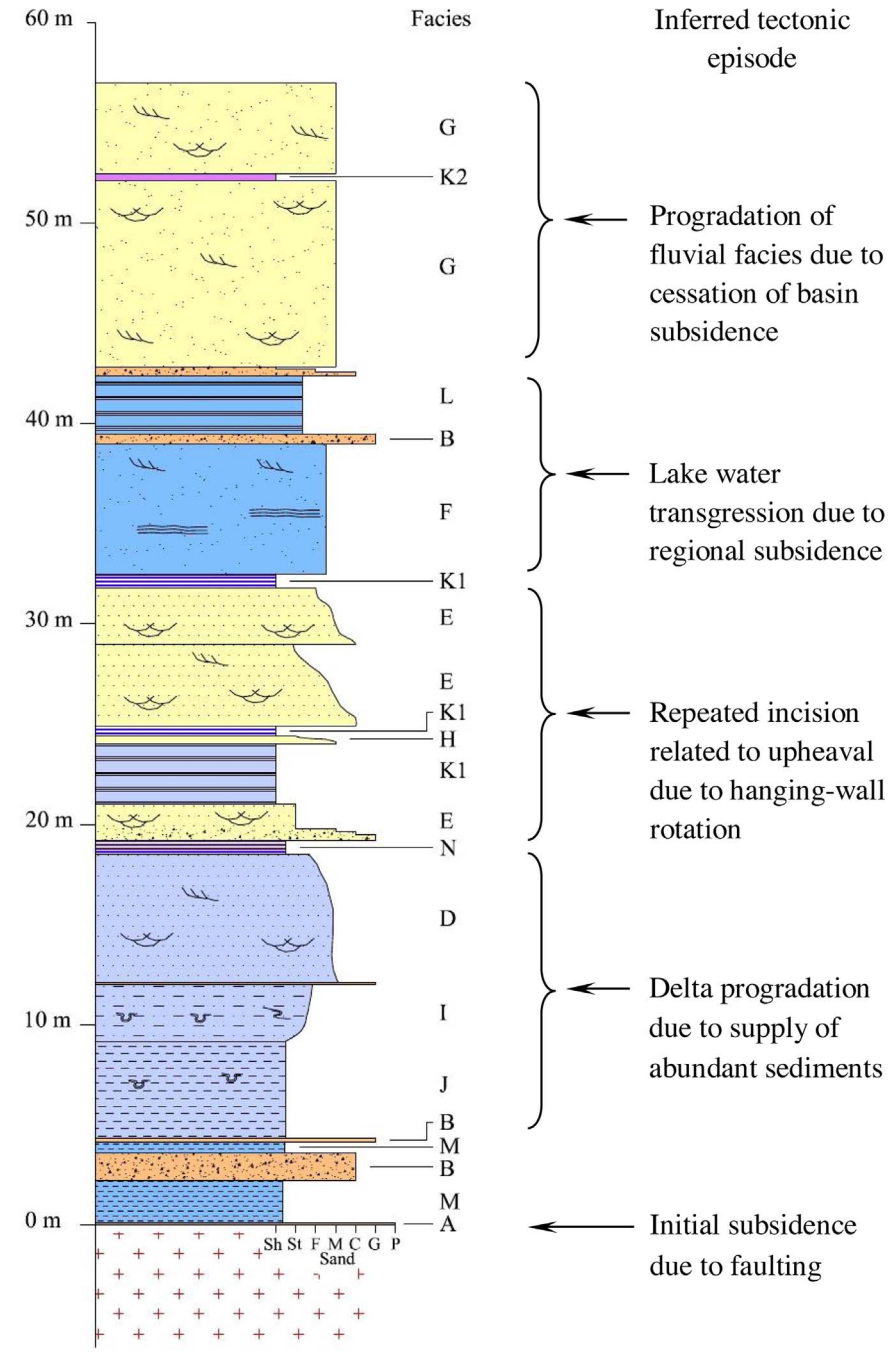

Fig. 2. Simplified and representative litholog depicting temporal disposition of different facies identified in the Srisailam Formation preserved in Chitrial outlier. Note the overall coarsening upward nature of the succession. Tectonic episodes as inferred from the mutual relationship of different recognized facies are also indicated.

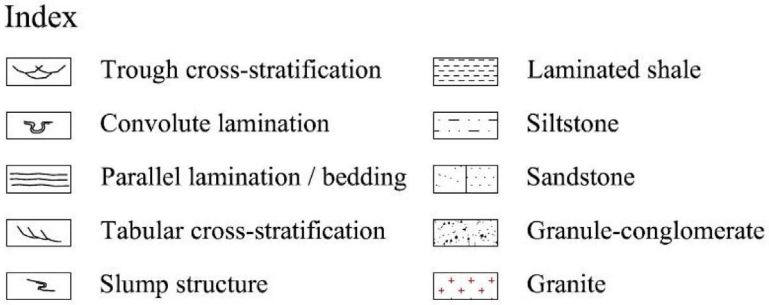

grained sandstone or silty-sandstone within thick (> 1 m) shale and silty-shale units were ignored while measuring thicknesses of shale units. Thicknesses of the 'black shale' units generally vary between 0.9 m and 18.0 m, but may go up to 29.0 m. However, in thicker sections intercalation of several millimeters of thin siltstone laminae is common. Sections (drill-core) containing both black and other shales are characterized by considerably high 'black shale' to 'total shale' ratio. 'Black shale' to 'total shale' ratio is generally > 0.51 but may be

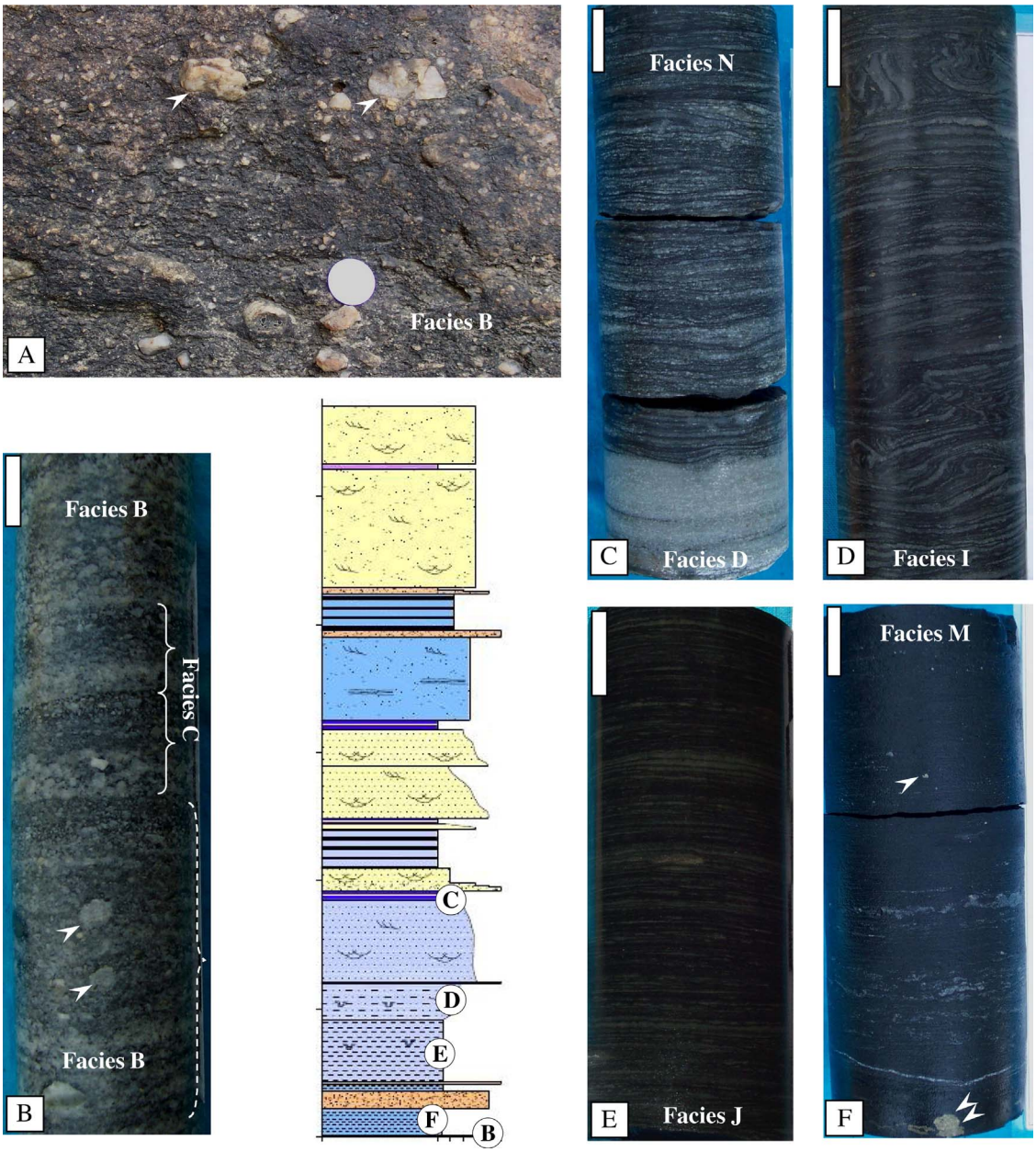

Fig. 3. (A) Field photograph of Facies B. Note the occurrence of outsized clasts (single arrow) in the middle of the facies. It suggests transportation by shear stress from the overlying turbulent layer (Dasgupta, 2003); (B) Photograph of core showing stacked couplets (shown with right braces) of granule-conglomerate to coarse-grained sandstone and medium-grained sandstone in Facies C sandwiched between Facies B; (C) Photograph of core showing the gradational contact between Facies D (mouthbar sandstone) and Facies N (interdistributary bay mudrock). Note the presence of wavy and thin lenticular bedding in Facies N; (D) Photograph of core showing synsedimentary deformation features like convolute laminations (in the upper part), slump structures (in the lower part) in Facies I (delta slope siltstone to fine sandstone); (E) Photograph of core showing thin, horizontally laminated, grey to dark-grey prodelta siltstone and shale (Facies J). Note the laterally discontinuous nature of the laminae and their diffused upper and lower contacts; (F) Photograph of core showing thin, horizontally laminated dark-grey/black deep lacustrine shale. Note the presence of solitary sand grains (single arrow) near top, and lump of pyrite (double arrows) near base. Diameter of the coin is 2.5 cm. The length of the scale bar is 2.0 cm. Encircled letters in the stratigraphic column indicate the positions of the core photographs.

as low as 0.21. Light-grey to dark-grey/black shale, silty-shale and siltstone units frequently contain pyrite in the form of fine disseminations, thin laminae or larger lumps.

On the basis of lithological attributes, sedimentary structures, and bed geometry of different lithological units fifteen different sedimentary facies have been recognized (Table 1). Causative sedimentary processes were inferred, combinations of the processes were established, and thereby depositional environments were reconstructed by recognizing five different facies associations (FA-I to V; Table 1). A representative litholog with most of the recognized facies is presented in Fig. 2.

The sedimentary succession of the Srisailam Formation in Chitrial outlier starts in general with the sediments of Facies A or B of FA-I (alluvial fan/fan-delta association; Table 1). They thin-out or pass into Facies C down-dip, and inside the basin underlie laminated dark-grey or black shale of deep lacustrine facies (Facies M of FA-IV). Facies M frequently rests directly over the basement granite inside the basin. However, locally thick wedges of Facies A or B are found (intercepted in borehole) directly over the basement granite well-inside the basin. The sediments of deep lacustrine facies are overlain successively by prodelta (Facies J), delta slope (Facies I), and mouthbar sediments (Facies D) of delta front facies association (FA-III, Fig. 2), or sediments of shallow (Facies L) and near-shore (Facies F) lacustrine facies of FA-IV. The delta channel sandstone (Facies E) of delta top facies association (FA-II) often

Table 2
Geochemical data of black shales from Chitrial outlier of the Srisailam Formation.

Sample No.	Group I												Group II					
	RGD11	RGD12	RGD13	RGD14	RGD15	RGD16	RGD17	CTR32	CTR37	CTR316	CTR325	CTR327	CTR339	CTR341	CTR353	CTR364	Average	PAAS
SiO_2	62.78	65.51	53.20	68.65	65.25	64.38	58.28	58.45	60.05	63.85	76.86	68.41	60.50	61.80	67.80	63.80	63.72 ± 5.40	62.80
TiO_2	0.40	0.44	0.51	0.31	0.37	0.31	0.37	0.44	0.37	0.30	0.14	0.26	0.61	0.68	0.57	0.55	0.41 ± 0.14	1.00
Al_2O_3	16.91	16.94	21.59	15.25	16.22	17.32	17.18	18.53	18.49	16.14	11.52	15.23	17.80	18.80	17.30	17.40	17.04 ± 2.12	18.90
FeO	1.26	1.08	0.99	1.17	1.26	0.90	1.35	1.17	1.08	1.08	0.54	0.99	1.80	1.40	1.80	1.40	1.20 ± 0.31	6.50
Fe_2O_3	3.51	2.55	4.46	1.78	2.66	2.43	6.22	4.36	3.82	3.84	1.27	2.17	5.90	5.00	3.00	5.90	3.68 ± 1.53	–
Fe_2O_3(T)	4.91	3.75	5.56	3.08	4.06	3.43	7.72	5.66	5.02	5.04	1.87	3.27	7.90	6.56	5.00	7.46	5.02 ± 1.76	–
MnO	0.01	0.01	0.01	0.01	0.01	0.01	0.01	0.01	0.01	0.01	0.01	0.01	< 0.01	< 0.01	< 0.01	0.01	0.01	0.11
MgO	1.02	1.02	1.11	0.67	0.85	0.70	1.23	1.19	1.04	0.83	0.41	0.62	1.60	1.20	0.90	1.00	0.96 ± 0.29	2.20
CaO	0.20	0.20	0.22	0.19	0.15	0.18	0.15	0.31	0.17	0.12	0.12	0.14	0.20	0.20	0.30	0.30	0.20 ± 0.06	1.30
Na_2O	0.52	1.05	0.72	1.30	0.71	1.04	0.93	0.84	0.88	0.89	1.00	1.07	1.10	1.00	1.20	0.60	0.93 ± 0.21	1.20
K_2O	5.97	5.87	7.09	5.66	5.73	6.50	6.00	6.64	6.94	5.88	4.21	5.47	0.60	0.70	0.60	0.60	4.65 ± 2.49	3.70
P_2O_5	0.05	0.03	0.06	0.04	0.04	0.03	0.06	0.15	0.05	0.04	0.02	0.03	0.04	0.03	< 0.01	0.03	0.05 ± 0.03	0.16
LOI	5.03	4.74	7.13	3.37	4.87	4.28	6.11	5.61	5.21	5.08	2.37	3.54	8.50	7.70	5.00	7.60	5.38 ± 1.68	6.00
Total	97.66	99.44	97.09	98.40	98.12	98.08	97.89	97.70	98.11	98.06	98.47	97.94	98.65	98.51	98.47	99.19	98.24 ± 0.58	99.90
C_{org}	0.64	0.81	0.74	0.75	1.10	0.70	0.62	0.69	0.57	0.55	0.45	0.69	na	na	0.74	0.82	0.71 ± 0.15	–
C_{tot}	0.68	0.81	0.75	0.77	1.10	0.70	0.62	0.70	0.59	0.55	0.49	0.69	na	na	0.74	0.83	0.72 ± 0.15	–
CIA	71	67	71	65	68	66	68	68	68	67	66	66	87	87	85	90	72 ± 9	70
PIA	95	84	91	81	88	84	87	89	89	86	84	83	89	90	87	93	87 ± 4	79
ICV	0.69	0.66	0.65	0.65	0.65	0.64	0.87	0.74	0.72	0.74	0.62	0.64	0.56	0.47	0.38	0.51	0.64 ± 0.12	0.89
SiO_2/Al_2O_3	3.71	3.87	2.46	4.50	4.02	3.72	3.39	3.15	3.25	3.96	6.67	4.49	3.40	3.29	3.92	3.67	3.84 ± 0.91	3.32
K_2O/Na_2O	11.48	5.59	9.85	4.35	8.07	6.25	6.45	7.90	7.89	6.61	4.21	5.11	0.55	0.70	0.50	1.00	5.41 ± 3.38	3.08
Al_2O_3/TiO_2	42	39	42	49	44	56	46	42	50	54	82	59	29	28	30	32	45 ± 14	18.9
K_2O/Al_2O_3	0.35	0.35	0.33	0.37	0.35	0.38	0.35	0.36	0.38	0.36	0.37	0.36	0.03	0.04	0.03	0.03	0.28 ± 0.15	0.20
CaO/Al_2O_3	0.01	0.01	0.01	0.01	0.01	0.01	0.01	0.02	0.01	0.01	0.01	0.01	0.01	0.01	0.02	0.02	0.01	0.07
Na_2O/Al_2O_3	0.03	0.06	0.03	0.09	0.04	0.06	0.05	0.05	0.05	0.06	0.09	0.07	0.06	0.05	0.07	0.03	0.06 ± 0.02	0.06
TiO_2/Zr	25	26	23	18	27	23	21	24	25	19	–	20	–	42	35	31	26 ± 6	48
Rb	231	246	298	200	182	174	240	256	220	192	110	160	na	na	na	na	209 ± 50	160
Sr	38	55	40	61	40	63	36	34	32	34	48	53	na	51	49	27	44 ± 11	200
Ba	633	646	780	690	653	719	488	519	508	446	429	565	na	440	504	352	558 ± 123	650
Zr	162	168	226	168	138	132	177	183	149	155	72	128	na	163	163	175	157 ± 33	210
Hf	< 10	< 10	< 10	< 10	< 10	< 10	< 10	< 10	< 10	< 10	< 10	< 10	< 10	< 10	< 10	< 10	–	5.0
Nb	45	14	26	< 10	12	< 10	14	17	21	< 10	< 10	< 10	na	11	20	70	25 ± 19	19
Ta	< 10	< 10	< 10	< 10	< 10	< 10	< 10	< 10	< 10	< 10	< 10	< 10	na	< 10	< 10	25	–	–
Th	36	27	42	18	24	22	48	56	48	42	10	20	na	13	18	20	30 ± 14	14.6
U	7	8	10	8	6	7	8	11	21	8	8	8	6	5	5	5	8 ± 4	3.1
Pb	29	29	27	27	23	17	42	36	34	27	15	23	na	22	< 10	12	26 ± 8	20
V	45	47	74	39	41	37	45	60	54	43	23	35	na	35	48	52	45 ± 12	150
Cr	120	138	157	157	198	170	114	125	101	84	52	97	na	93	99	100	120 ± 38	110
Ni	32	40	68	21	26	94	66	77	45	38	15	32	na	24	20	34	42 ± 23	55
Cu	32	30	53	18	20	20	36	28	24	22	16	20	na	20	13	18	25 ± 10	50
Zn	63	51	46	32	95	38	57	72	93	55	38	27	na	54	27	57	54 ± 21	85
Sc	12	12	16	9	12	10	13	15	15	12	6	10	2	2	2	2	9 ± 5	16
Y	15	16	23	13	13	13	20	29	20	18	6	14	23	21	19	19	18 ± 5	27
La	23	27	49	22	12	16	42	49	48	40	15	25	42	35	26	33	32 ± 12	38
Ce	49	48	99	40	29	33	70	92	90	81	30	41	83	69	49	67	61 ± 24	80
Pr	< 10	< 10	< 10	< 10	< 10	< 10	< 10	< 10	< 10	< 10	< 10	< 10	< 10	< 10	< 10	< 10	–	8.9
Nd	20	19	38	20	18	17	28	37	33	32	10	18	42	35	26	33	27 ± 9	32
Sm	6	6	8	5	5	6	7	9	8	7	3	5	6	5	6	5	6 ± 1	5.6
Eu	0.4	0.5	0.6	0.3	0.5	0.5	0.5	1.0	1.2	0.7	0.3	0.5	0.8	0.6	0.5	0.5	0.6 ± 0.2	1.1
Gd	4	4	6	4	3	3	5	8	6	5	< 2	3	8	7	5	7	5 ± 2	4.7
Tb	< 2	< 2	< 2	< 2	< 2	< 2	< 2	< 2	< 2	< 2	< 2	< 2	< 2	< 2	< 2	< 2	–	0.77
Dy	3	3	4	3	2	3	4	6	4	4	< 2	< 2	3	3	3	3	3 ± 1	4.4

(*continued on next page*)

Table 2 (*continued*)

Sample No.	Group I											Group II				Average	PAAS
	RGD11	RGD12	RGD13	RGD14	RGD15	RGD16	RGD17	CTR32	CTR37	CTR316	CTR325	CTR327	CTR339	CTR341	CTR353	CTR364		
Ho	< 2	< 2	< 2	< 2	< 2	< 2	< 2	< 2	< 2	< 2	< 2	< 2	< 2	< 2	< 2	< 2	–	1.0
Er	< 2	< 2	< 2	< 2	< 2	< 2	< 2	< 2	< 2	< 2	< 2	< 2	4	3	< 2	3	3 ± 1	2.9
Tm	< 2	< 2	< 2	< 2	< 2	< 2	< 2	< 2	< 2	< 2	< 2	< 2	< 2	< 2	< 2	< 2	–	0.40
Yb	2.9	2.0	3.3	2.0	1.4	1.8	2.8	3.0	2.7	2.5	0.4	0.6	2.4	2.2	2.0	2.2	2.1 ± 0.8	2.8
Lu	0.4	0.3	0.4	0.3	0.3	0.3	0.4	0.5	0.4	0.4	0.1	0.1	0.5	0.5	0.5	0.5	0.4 ± 0.1	0.43
ΣREE	108.7	109.8	208.3	96.6	69.2	77.6	159.7	205.5	193.3	172.6	58.8	93.2	191.2	159.8	117.5	153.7	136.0 ± 50.4	183.0
La_{CN}/Yb_{CN}	5.36	9.12	10.03	7.43	5.79	6.01	10.14	11.04	12.01	10.81	25.34	28.16	11.83	10.75	8.78	10.14	11.42 ± 6.36	9.17
La_{CN}/Sm_{CN}	2.41	2.83	3.86	2.77	1.51	1.68	3.78	3.43	3.78	3.60	3.15	3.15	4.41	4.41	2.73	4.15	3.23 ± 0.87	4.27
Gd_{CN}/Yb_{CN}	1.12	1.62	1.47	1.62	1.74	1.35	1.45	2.16	1.80	1.62	2.03	4.05	2.70	2.58	2.03	2.58	1.99 ± 0.72	1.36
Eu/Eu*	0.25	0.31	0.26	0.20	0.39	0.36	0.26	0.36	0.53	0.36	0.53	0.39	0.35	0.31	0.28	0.26	0.34 ± 0.09	0.66
Th/U	5.14	3.38	4.20	2.25	4.00	3.14	6.00	5.09	2.29	5.25	1.25	2.50	–	2.60	3.60	4.00	3.65 ± 1.34	4.71
La/Sc	1.9	2.3	3.1	2.4	1.0	1.6	3.2	3.3	3.2	3.3	2.5	2.5	21.0	17.5	13.0	16.5	6.1 ± 6.7	2.4
La/Cr	0.19	0.20	0.31	0.14	0.06	0.09	0.37	0.39	0.48	0.48	0.29	0.26	–	0.38	0.26	0.33	0.28 ± 0.13	0.35
Th/Sc	3.00	2.25	2.63	2.00	2.00	2.20	3.69	3.73	3.20	3.50	1.67	2.00	–	6.50	9.00	10.00	3.82 ± 2.60	0.91
Th/Cr	0.30	0.20	0.27	0.11	0.12	0.13	0.42	0.45	0.48	0.50	0.19	0.21	–	0.14	0.18	0.20	0.26 ± 0.14	0.13
La/Y	1.5	1.7	2.1	1.7	0.9	1.2	2.1	1.7	2.4	2.2	2.5	1.8	1.8	1.7	1.4	1.7	1.8 ± 0.4	1.4
Ce/Sc	4.1	4.0	6.2	4.4	2.4	3.3	5.4	6.1	6.0	6.8	5.0	4.1	41.5	34.5	24.5	33.5	12.0 ± 13.2	5.0

Major oxides, C_{org} and C_{tot} are in wt.%, trace elements are in ppm; PAAS, Post-Archaean average Australian shale (Taylor and McLennan, 1985); CIA, Chemical Index of Alteration (Nesbitt and Young, 1982); ICV, Index of Compositional Variability (Cox et al., 1995); PIA, Plagioclase Index of Alteration (Fedo et al., 1995); CN, Chondrite-normalized. Chondrite normalizing values are from Taylor and McLennan (1985). $Eu/Eu^* = Eu_{CN}/(Sm_{CN}*Gd_{CN})^{0.5}$ after Taylor and McLennan (1985). na, not analyzed.

show stacked repetition (Fig. 2). The delta front and delta top sediments are also overlain successively by shallow (Facies L) and near-shore (Facies F) lacustrine facies sediments. Sheet-like body of laterally amalgamated sediments of fluvial facies association (FA-V) cap the sediments of all other facies associations. The identified facies of the Srisailam Formation, except for those of FA-V, show frequent changes in vertical stacking pattern and thickness.

5. Whole-rock geochemistry

5.1. Materials and methodology

Sixteen representative samples of carbonaceous-shale, -mudstone, and -silty-shale (hereafter 'black shale' *sensu lato*) of Facies J and M were collected for geochemical study during the course of subsurface exploration for unconformity-associated uranium mineralization in Chitrial outlier (Fig. 1c; Fig. S4) by Atomic Minerals Directorate for Exploration and Research (AMD). The samples (200–300 g) were first washed thoroughly with water to avoid any contamination from cutting slimes and oil, and then dried and powdered to −200# (74 μ) for chemical analysis at the Chemical laboratory, AMD, Hyderabad. Among the major oxides, SiO_2, TiO_2, and P_2O_5 were analyzed by spectrophotometry; FeO by redox titrimetry (Pratt's method); K_2O and Na_2O by flame-photometry; loss-on-ignition (LOI) by gravimetry, and the remaining major oxides by Atomic Absorption Spectrometry (AAS). For estimating LOI 1.0 gm of powdered sample was heated at 950 °C in a muffle furnace for ~2 h. LOI was calculated by measuring the difference in weight of the sample before and after heating, and expressed in percentage. Total carbon (C_{tot}) and organic carbon (C_{org}) were determined by carbon analyzer (Liqui TOC II, Elementar, Germany) precalibrated using soil (4.1 wt.% C_{org}) standard. The trace elements and rare earth elements (REEs) were analyzed by Inductively Coupled Plasma-Optical Emission Spectrometry (ICP-OES, ULTIMA 2, France; equipped with dual grating and optics with 1 m focal length). The standard solutions, prepared using pure (99.99999% purity) chemical oxides/elements (Johnson and Matthey, UK), were used for calibration of the instruments. Certified reference material of carbonaceous shale (SARM-41, SA Bureau of Standards, South Africa) was analyzed simultaneously for accuracy. Replicate analysis of selected samples indicated better than 2% precision for analysis of major oxides, and 5–10% for the elements analyzed by ICP-OES and carbon analyzer. The major oxide, trace element, and REE concentrations are presented in Table 2.

5.2. Major oxides

The major oxides of the Srisailam black shales show considerable variations. SiO_2 abundances are broadly similar to that of post-Archaean average Australian shale (PAAS; Taylor and McLennan, 1985) with majority (n = 14) of the samples lying within ± 10% of it (Table 2). Though SiO_2 ranges from 53.20 wt.% (RGD13) to 76.86 wt.% (CTR325), most of the samples (n = 14) fall in a narrower range of 58–69 wt.%. Similarly, Al_2O_3 contents vary widely, but majority (n = 14) of the samples contain 15–19 wt.%. Except for one (RGD13, 21.59 wt.%), the samples are variably depleted in Al_2O_3 compared to PAAS (18.90 wt.%). The samples in SiO_2–Al_2O_3 plot (Fig. 4a) fall on a line that intercepts the ordinate at ~100 wt.% SiO_2. SiO_2/Al_2O_3 ratios of the samples are close to that of PAAS (3.32), with majority (n = 14) of them being within the range 3.15–4.50. One sample (CTR325, carbonaceous silty-shale) show considerably high SiO_2/Al_2O_3 ratio (6.67). The Srisailam black shales are strongly depleted in TiO_2 compared to PAAS. TiO_2 contents vary considerably with majority (n = 12) of the samples lying within the range 0.30–0.57 wt.%. It shows moderate positive correlation (r = 0.71) with Al_2O_3. Fe_2O_3(T) contents in the samples range between 1.87 and 7.90 wt.%, and show moderate positive correlation (r = 0.61) with Al_2O_3. Similarly, MgO with general low

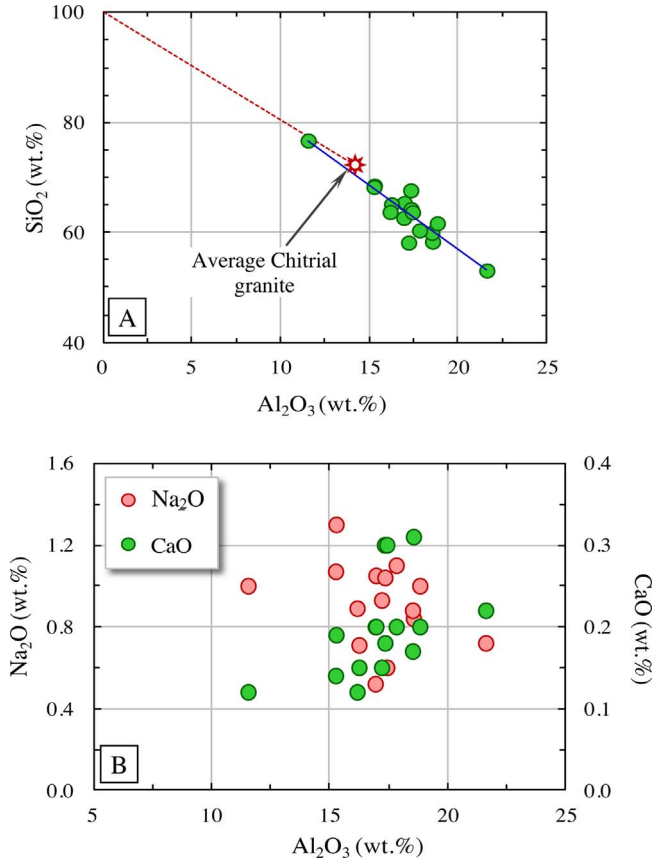

Fig. 4. (A) Al_2O_3–SiO_2 plot showing the effect of quartz dilution on the Srisailam black shales. This also indicates that Al_2O_3 was not affected by hydraulic sorting and chemical alteration (Fralick, 2003). Dashed line is the ideal weathering path (considering average Chitrial granite as the source rock) indicating immobility of Al_2O_3. Minor scattering is due to compositional variation in source rock(s); (B) Plots of the Srisailam black shales in Al_2O_3–Na_2O/Al_2O_3–CaO bivariate space. Note the lack of any correlation of Na_2O and CaO with Al_2O_3.

abundances shows moderate positive correlation (r = 0.70) with Al_2O_3. Among other major oxides the abundances of Na_2O and CaO are significantly lower than PAAS. They do not show any correlation with Al_2O_3 (Fig. 4b). K_2O contents as well as K_2O/Na_2O and K_2O/Al_2O_3 ratios vary widely, and they show distinct bimodality (Table 2). LOI varies from 2.37–8.50 wt.%, and shows moderate positive correlation (r = 0.74) with Al_2O_3. Total carbon (0.49 − 1.10 wt.%, Av. 0.72 ± 0.15 wt.%) and organic carbon (0.45 − 1.10 wt.%, Av. 0.71 ± 0.15 wt.%) concentrations show restricted range (Table 2).

Chemical Index of Alteration (CIA; Nesbitt and Young, 1982) and Plagioclase Index of Alteration (PIA; Fedo et al., 1995) are the most widely used chemical indices in geochemical study of sedimentary rocks for quantifying source-area weathering. PIA helps in monitoring the weathering of plagioclase alone (Fedo et al., 1995). The CIA values of the samples, though vary widely (65–90, Av. 72 ± 9), the PIA values (81–95, Av. 87 ± 4) show relatively restricted range. Index of Compositional Variability (ICV; Cox et al., 1995) in the Srisailam black shales ranges from 0.38 (CTR353) to 0.87 (RGD17) with an average of 0.64 ± 0.12.

5.3. Trace elements

The average Srisailam black shale is enriched in Rb, Cr, and Pb, and depleted in Sr, Ba, Sc, V, Ni, Cu, and Zn compared to PAAS. Nb and Sc show bimodality (Table 2). Rb (r = 0.89) shows strong positive correlation with Al_2O_3, while Sr (r = −0.28) and Ba (r = 0.29) do not show any correlation. Zr and Y are depleted compared to both PAAS and Upper Continental Crust (UCC; Taylor and McLennan, 1985), whereas Th and U are enriched compared to both of them (Table 2). Among HFSEs, Zr (r = 0.85), Y (r = 0.80), La (r = 0.68), and Ce (r = 0.72) show strong to moderate positive correlation with Al_2O_3. Weak positive correlation exists between Th (r = 0.51) and Al_2O_3, while Sc (r = 0.23), Nb (r = 0.32), U (r = 0.21), and Pb (r = 0.26) do not show any correlation. Amongst the transition metals, only V shows strong (r = 0.83), Cu moderate (r = 0.63), and Ni weak positive correlation (r = 0.52) with Al_2O_3. Cr (r = 0.36) and Zn (r = 0.28) do not show any correlation with Al_2O_3.

5.4. Rare earth elements (REEs)

The REE abundances in the Srisailam black shales vary moderately (Table 2). Total REE abundances (ΣREE) range from 59 to 208 ppm with an average (136.0 ± 50.4 ppm) comparable to that of UCC (146.4 ppm; Taylor and McLennan, 1985) but considerably lower than that of PAAS (183.0 ppm; Taylor and McLennan, 1985). ΣREE shows moderate positive correlation (r = 0.74) with Al_2O_3. The samples have considerably variable La_{CN}/Yb_{CN} (5.36–28.16), La_{CN}/Sm_{CN} (1.51–4.41), and Gd_{CN}/Yb_{CN} (1.12–4.05) ratios, but chondrite-normalized REE patterns (Fig. 5a and b) of most of the samples are broadly similar to that of PAAS. Though the average La_{CN}/Yb_{CN} ratio (11.42) depicts more fractionated pattern than PAAS (9.17) and UCC (9.21), LREE pattern (Av. La_{CN}/Sm_{CN}, 3.23) is considerably flatter (Fig. 5b) than both of them (4.27 and 4.20 respectively). All the samples are

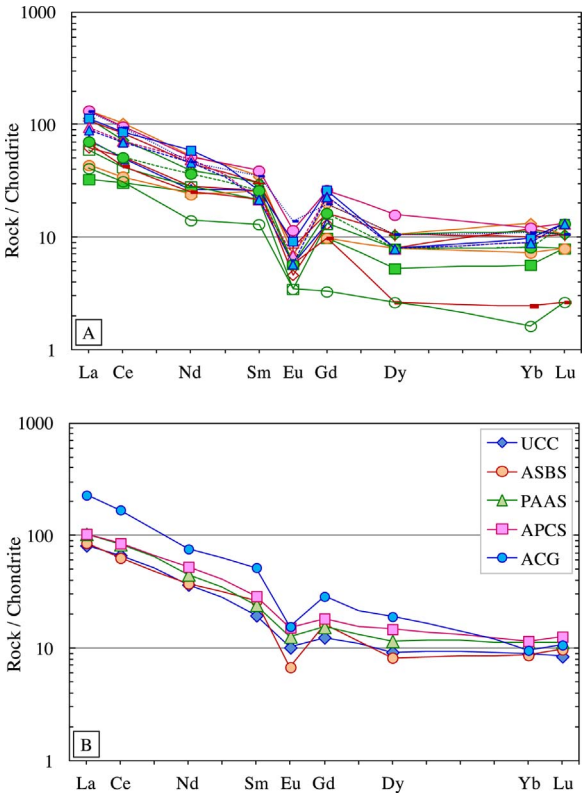

Fig. 5. (A) Chondrite-normalized REE patterns of the Srisailam black shales. Normalizing values are after Taylor and McLennan (1985). $Eu/Eu^* = Eu_{CN}/(Sm_{CN}*Gd_{CN})^{0.5}$ after Taylor and McLennan (1985). Pr_{CN} is calculated as $(Ce_{CN}*Nd_{CN})^{0.5}$ and Tb_{CN} as $(Gd_{CN}*Dy_{CN})^{0.5}$. Values of Ho_{CN}, Er_{CN}, and Tm_{CN} are calculated from the slope of the line joining Dy_{CN} and Yb_{CN}; (B) Comparison of chondrite-normalized pattern of the average Srisailam black shale (ASBS) with post-Archaean average Australian shale (PAAS; Taylor and McLennan, 1985), upper continental crust (UCC; Taylor and McLennan, 1985), and average Proterozoic cratonic shale (APCS; Condie 1993). Note the more pronounced negative Eu-anomaly in the Srisailam black shale. REE pattern of the average Chitrial granite (ACG, n = 24) is also presented for comparison. Note the similarity of the overall REE pattern and Eu-anomaly of the average Srisailam black shale (ASBS) with it.

Table 3
Ranges of provenance indicator critical trace elemental ratios in the Srisailam black shales.

Ratios	Range in sediment† from silicic sources	Range in sediment† from basic sources	Range in Srisailam black shales	PAAS	UCC
Eu/Eu*	0.32–0.83	0.70–1.02	0.20–0.53	0.66	0.65
La/Sc	0.7–27.7	0.4–1.1	1.0–21.0	2.4	2.7
Th/Sc	0.64–18.10	0.05–0.40	1.67–10.00	0.91	0.97
Th/Cr	0.067–4.00	0.002–0.045	0.11–0.50	0.13	0.31

†Data on the same ratios for finer sediments derived from granitoids and basic sources (from Cullers, 2000) are also given for comparison. UCC (upper continental crust) and PAAS (post-Archaean average Australian shale) data are from Taylor and McLennan (1985).

characterized by more conspicuous negative Eu-anomaly (Eu/Eu*, 0.20–0.53, Table 2; Fig. 5a) than both PAAS and UCC (0.66 and 0.65 respectively; Taylor and McLennan, 1985).

5.5. Elemental ratios

Some trace elemental ratios viz. La/Sc, Th/Sc, Th/Cr, and Eu/Eu* (Cullers, 2000) are often critically more representative of source rocks of detrital sediments. The ranges of these provenance indicator critical trace elemental ratios in the Srisailam black shales are presented in Table 3. La/Sc and Th/Sc ratios show bimodal distribution, and higher average values [La/Sc (2.6x PAAS), Th/Sc (4.2x PAAS)] than PAAS. Th/Cr ratios show considerably restricted range (0.11–0.50) and higher average value (2.0x PAAS) than PAAS. In contrast, the black shales are characterized by lower average Eu/Eu* ratio (0.52x PAAS) than PAAS.

Th/U ratio of siliciclastic rocks may be useful in interpreting sedimentary recycling history, intensity of chemical weathering (McLennan et al., 1990), and differentiating aeolian depositional environments from fluvial and shallow marine environments (Basu et al., 2009). The Th/U ratio of the UCC is 3.82 (Taylor and McLennan, 1985). Th is mainly transported as solid particulate load, and because of remarkable stability in sedimentary environment quantitative transfer of Th takes place from provenance to basin (Basu et al., 2009 and references therein). During chemical weathering and aqueous sedimentation under oxidizing condition U is readily oxidized to soluble U^{6+} and goes into solution. This increases the Th/U ratio in sediments (McLennan et al., 1990). However, authigenic enrichment of U in mudrocks, deposited under anoxic to dysoxic bottom water condition, may lower the Th/U ratio. The Th/U ratios (Table 2) in the samples range between 1.25 and 6.00 with considerable lower average value (Av. 3.65 ± 1.34; 0.8x PAAS) than PAAS (4.71). However, the average Th/U ratio of the black shales is only marginally lower (0.95x UCC) than that of UCC due to nominal authigenic enrichment of U (Av. 0.6 ppm).

5.6. Geochemical grouping of the samples

The samples in hand specimen, drill-core, and surface exposures apparently show comparable lithological characteristics (viz. colour, grain size, and texture). However, on the basis of geochemical data, especially K_2O contents, and K_2O/Na_2O and K_2O/Al_2O_3 ratios, the samples have been divided into two distinct groups [hereafter Group I (n = 12) and II (n = 4); Fig. 6a and b; Table 2]. The Group I samples are characterized by significantly higher K_2O (4.21–7.09 wt.%, Av. 6.00 ± 0.76 wt.%), K_2O/Na_2O (4.21–11.48, Av. 6.98 ± 2.18), and K_2O/Al_2O_3 (0.33–0.38, Av. 0.36 ± 0.01) ratios than PAAS (3.70 wt.%, 3.08, and 0.20 in the indicated order). In contrast, the Group II samples are characterized by significantly lower K_2O (0.60–0.70 wt.%, Av. 0.63 ± 0.05 wt.%), K_2O/Na_2O (0.50–1.00, Av. 0.69 ± 0.23), and K_2O/Al_2O_3 (0.03–0.04, Av. 0.035 ± 0.002) ratios than PAAS. However, strong positive correlation (Fig. 6b) exists between K_2O and Al_2O_3

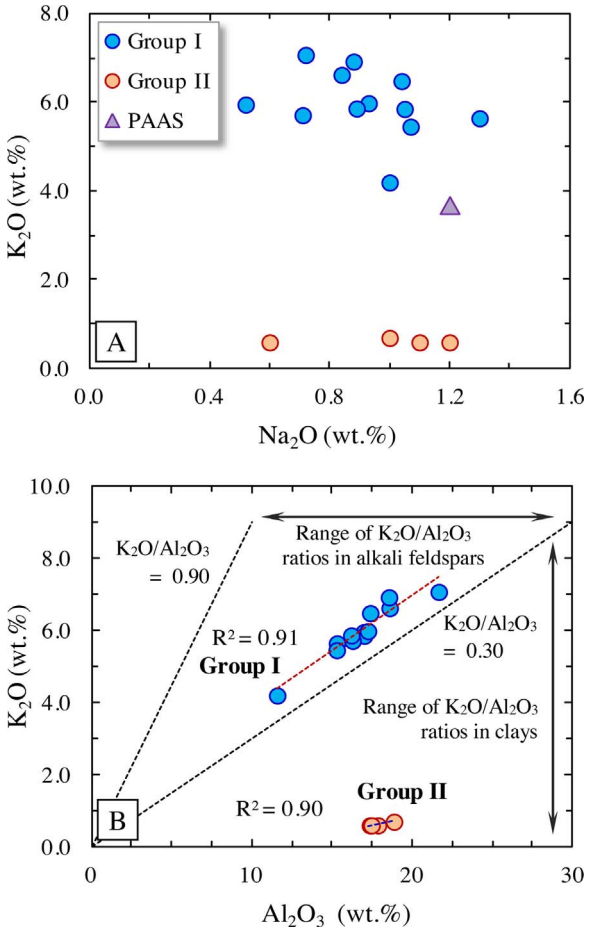

Fig. 6. (A) Plots of the Srisailam black shales in Na_2O–K_2O bivariate space. Note the clustering of the samples in two distinct groups. Post-Archaean average Australian shale (PAAS; Taylor and McLennan, 1985) is also plotted for reference; (B) Distinct clustering of the Srisailam black shales in two groups in Al_2O_3–K_2O plot. This also illustrates the variation in original mineralogical composition of the Srisailam black shales. Ranges of K_2O/Al_2O_3 in alkali feldspars and clays are from Cox et al. (1995).

in both the groups. Though the abundances of most of the trace elements show overlapping range, Sc abundances are distinctly higher in Group I (Av. 12 ppm) than Group II (Av. 2 ppm) samples.

The CIA values of Group I samples are distinctly lower (65–71, Av. 67 ± 2) than Group II (85–90, Av. 87 ± 2; Table 2) samples. However, the PIA values are comparable in both the groups. PIA varies between 81 and 95 (Av. 87 ± 4) in Group I, and between 87 and 93 (Av. 90 ± 2; Table 2) in Group II shales. Further, Group I samples have contrastingly higher ICV values (0.62–0.87, Av. 0.69 ± 0.07) than Group II (0.38–0.56, Av. 0.48 ± 0.08) samples. High ICV values (> 0.60) indicate dominance of alkali feldspar over clays (Cox et al., 1995) in Group I samples. In contrast, ICV values of Group II samples indicate dominance of plagioclase (Cox et al., 1995) in them.

6. Discussion

6.1. Source rock composition

There are a number of ways of inferring the provenance composition from the chemical composition of finer siliciclastics (Cullers and Podkovyrov, 2000). However, the nature and composition of the source rocks is best ascertained on the basis of concentrations of immobile and conservative elements viz. Al_2O_3, TiO_2, Zr, Th, Sc, and REEs in siliciclastic rocks (Taylor and McLennan, 1985; Hayashi et al., 1997). Being immobile in natural sedimentary environments Al_2O_3, TiO_2, REEs, Th,

Zr, and other HFSEs (Nb, Ta, Hf, and Y) are quantitatively transferred as detrital load from the source rocks (Taylor and McLennan, 1985; Hayashi et al., 1997). Plotting of Al_2O_3 of the black shale samples on a linear array that intercepts the ordinate at ~100 wt.% SiO_2 indicates that Al_2O_3 was not affected by hydraulic sorting or chemical alteration, and behaved as immobile element (Fralick, 2003). Moderate to strong positive correlation of TiO_2 (r = 0.71), Zr (r = 0.85), and ΣREE (r = 0.74) with Al_2O_3 indicates that these elements were not affected by hydraulic sorting and sedimentary recycling, and quantitatively transferred from source rocks. Moderate to strong positive correlation of Th (r = 0.71) and Sc (r = 0.92) with Al_2O_3 in Group I samples also reflects their quantitative transfer from source rocks. However, the black shales as a whole show weaker correlation of Th (r = 0.51) and no correlation of Sc (r = 0.23) with Al_2O_3 apparently due to relatively Th-poor and Sc-depleted nature of the Group II samples. The Group II shales are characterized by lower abundances of Th (Av. 17.0 ± 3.6 ppm, n = 3) and Sc (Av. 2.0 ppm). Since both Th and Sc are immobile over the entire sedimentary realm and diagenesis (Taylor and McLennan, 1985; Cullers, 2000), their lower abundances (favouring overall weaker correlation of Th and Sc with Al_2O_3) are inferred to be related to characteristics of the source rocks (discussed below) from which the Group II shales were derived. Further, the abundance of Zr (i.e., provenance signature) in siliciclastic rocks is often influenced by hydraulic sorting, grain-size-dependent fractionation, recycling, and aeolian input of sediments (McLennan et al., 1990; McLennan et al., 2003). McLennan et al. (2003) have shown that Zr/Sc ratio gradually increases at near-constant Th/Sc ratio due to sedimentary sorting and recycling processes, and in Th/Sc–Zr/Sc bivariate field this is manifested by sharp departure of plots from the trend observed with increasing igneous differentiation process (Fig. S5). In Th/Sc–Zr/Sc bivariate plot, the Srisailam black shales do not show any evidence of Zr enrichment due to sorting and recycling processes. Taylor et al. (1983) noted exceptionally high Zr in loess due to zircon enrichment during aeolian transportation. Marginally higher La/Zr ratio (Av. 0.19 ± 0.06, n = 15) of the black shales than UCC (0.16; Taylor and McLennan, 1985) indicates no aeolian input of zircon during sedimentation. Therefore, the geochemical characteristics indicate that Al_2O_3, TiO_2, Zr, Th, Sc, and REE abundances in finer siliciclastics of the Srisailam Formation portray the near-original source rock signatures.

Hayashi et al. (1997) observed that mafic igneous rocks are characterized by TiO_2/Zr weight ratio of > 195, intermediate igneous rocks between 195 and 55, and felsic igneous rocks by < 55. They devised a scheme for discriminating the source of the sedimentary rocks on the basis of TiO_2/Zr weight ratios. As per that discriminating scheme, the TiO_2/Zr weight ratios of the black shale samples (18–42, Av. 26 ± 6) indicate felsic igneous source rock (Fig. 7a). Lower TiO_2 abundances (Av. 0.41 ± 0.14 wt.%) compared to PAAS (1.0 wt.%) are also suggestive of evolved (felsic) source rock.

Al_2O_3/TiO_2 ratio is another important indicator of the provenance composition (Hayashi et al., 1997). Al_2O_3/TiO_2 weight ratio in igneous rocks generally shows a well-defined trend and normally increases from 3 − 8 in mafic igneous rocks, through 8 − 21 in intermediate igneous rocks, to 21 − 70 in felsic varieties (Hayashi et al., 1997). The Al_2O_3/TiO_2 ratios of the Srisailam black shales range between 28 and 82 (Av. 43 ± 10 excluding outlier value 82) suggesting their derivation from felsic igneous source rocks. The plots of the black shale samples in the Al_2O_3–TiO_2 bivariate space (Fig. 7b; McLennan et al., 1979; Schieber, 1992) clearly suggest granite-granodiorite (granite for Group I, and granodiorite for Group II shales) source rock for the Srisailam black shales.

REEs, Th, Sc, and other HFSEs are the most useful for monitoring the source area composition (Taylor and McLennan, 1985; McLennan and Taylor, 1991) as they are relatively immobile during weathering (Cullers, 2000), transportation, diagenesis, and metamorphism (Taylor and McLennan, 1985). REE pattern is considered to be representative of the provenance (Taylor and McLennan, 1985). Furthermore, the trace elemental ratios, especially La/Sc, Th/Sc, Th/Cr, and Eu/Eu*, are critical of provenance composition (Cullers, 2000; Cullers and Podkovyrov, 2000). Th/Sc is particularly sensitive to average provenance composition (McLennan et al., 1990). These ratios (Table 3) indicate felsic source rocks for the Srisailam black shales. A similar inference can also be drawn from the REE data. It is well established that REE patterns of siliciclastic rocks reflect average composition of the provenance (McLennan, 1989). The Srisailam black shales show fractionated REE pattern (La_{CN}/Yb_{CN}, 5.36–28.16, Av. 11.42 ± 6.36) and distinctly negative Eu-anomaly (Eu/Eu*, 0.20–0.53, Av. 0.34 ± 0.09; Fig. 5a and b). They also show moderately fractionated LREE pattern (Av. La_{CN}/Sm_{CN}, 3.23 ± 0.87) and relatively flat HREE pattern (Av. Gd_{CN}/Yb_{CN}, 1.99 ± 0.72). These characteristics along with more conspicuous negative Eu-anomaly compared to PASS (0.66) are suggestive of derivation of the sediments from a more differentiated upper crustal material (granitoids) than that from which PAAS derived. At present, granodiorites with similar negative Eu-anomaly (0.28–0.76) are found exposed northeast of Peddavoora schist belt (Vimal et al., 2012), and differentiated granites (Eu/Eu*, 0.20–0.76) along all other sides of Chitrial outlier (Fig. 1c).

Another interesting feature is that though near-half of the samples (n = 9) have relatively flat HREE pattern, the remaining samples (n = 7) have Gd_{CN}/Yb_{CN} ratio > 2 (Fig. 8). Such high Gd_{CN}/Yb_{CN} ratios are characteristic of Archaean turbidites (McLennan and Taylor, 1991), or sediments derived from Archaean Na-rich igneous rocks viz. tonalite, trondhjemite, and granodiorite (McLennan et al., 1990; McLennan and Taylor, 1991). These samples therefore indicate a different source from the others (showing Gd_{CN}/Yb_{CN} ratio < 2), or may be attributed to sedimentological processes viz. mixing of sediments from different sources, hydraulic sorting. Four of these samples, which plot in 'granodiorite' field in source-rock-discriminating Al_2O_3–TiO_2 bivariate space (Fig. 7b), belong to Group II shales. Nevertheless, the Group II samples are characterized by low Na_2O (0.98 ± 0.26 wt.%) and Sc (Av. 2 ppm) contents. Further, they show strong negative Eu-anomaly (0.26–0.35, Av. 0.30 ± 0.04) unlike sediments derived from Archaean Na-rich igneous rocks (> 0.85; McLennan and Taylor, 1991). It is therefore likely that the granodiorite suite of rocks, from which the Group II shales derived, was affected by hydrothermal alteration event(s) prior to weathering and erosion. The hydrothermal event(s) caused widespread alteration of especially plagioclase, enhanced Eu/Eu* anomaly, and depleted Sc due to alteration of ferromagnesian minerals. Vimal et al. (2012) observed frequent alteration of plagioclase to sericite, and hornblende to chlorite in TGA suite of rocks occurring northeast of Peddavoora schist belt (Fig. 1c). Significant removal of K_2O and especially Na_2O from this sericitized granodiorite suite of rocks even during moderate degree of chemical weathering (as indicated by CIA of Group I shales) was responsible for K- and Na-depleted nature of the Group II shales. Esmaeili and Afshouni (2009) observed depletion of Sc in hydrothermally altered granodiorite of Astaneh massif, Iran. Parsapoor et al. (2015) noted a sharp drop of Eu/Eu* in sericitic zone of granodiorite porphyry Cu-deposit, Darreh-Zar, Iran. The remaining three samples, which plot in 'granite' field in source-rock-discriminating Al_2O_3–TiO_2 bivariate space (Fig. 7b), belong to Group I shales. The overlapping Al_2O_3/TiO_2 ratio and REE signature of these samples indicate mixing of sediments from different sources, or hydraulic sorting of heavy minerals (viz. zircon). Very high La_{CN}/Yb_{CN} ratios (25.34 and 28.16 respectively) in two of these samples distinctly support mixing of sediments from different sources (Taylor and McLennan, 1985). Marginally higher La/Zr ratios (0.21 and 0.20) than UCC (0.16) in these samples indicate that hydraulic sorting might also have contributed to a lesser extent. Therefore, the Group I shales were dominantly derived from granite, and the Group II shales were derived from granodiorite (TGA; Vimal et al., 2012) source rocks.

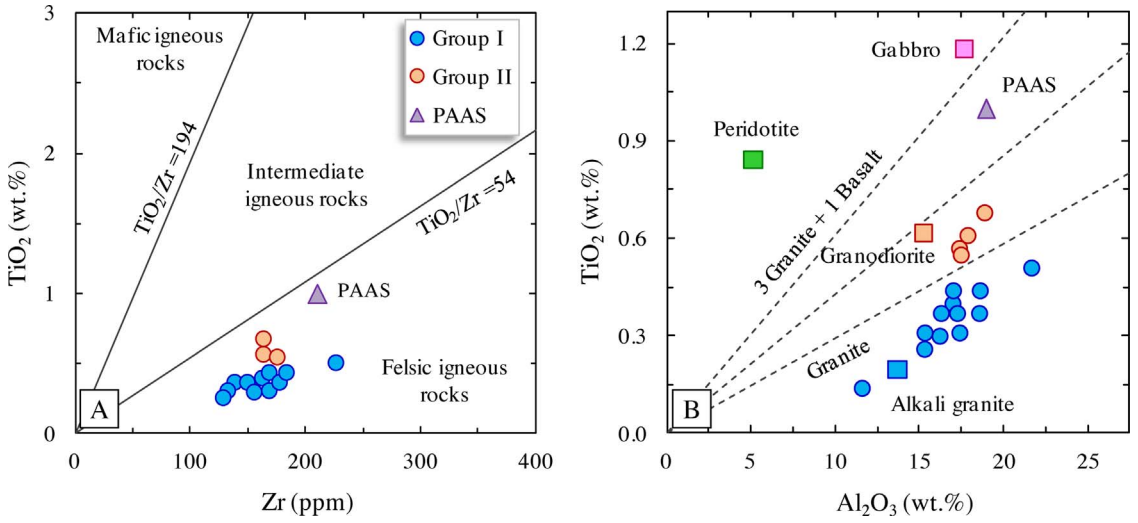

Fig. 7. (A) TiO_2–Zr discrimination plots indicating felsic igneous source rocks for the Srisailam black shales. TiO_2–Zr discriminating field values are after Hayashi et al. (1997); (B) Al_2O_3–TiO_2 bivariate space (after McLennan et al., 1979) suggesting granite-granodiorite source rock for the Srisailam black shales. The 'granite line' and the '3 granite + 1 basalt line' are from Schieber (1992). Post-Archaean average Australian shale (PAAS; Taylor and McLennan, 1985) is also plotted for reference. Plots of granodiorite, gabbro, peridotite, and alkali granite are after Paikaray et al. (2008).

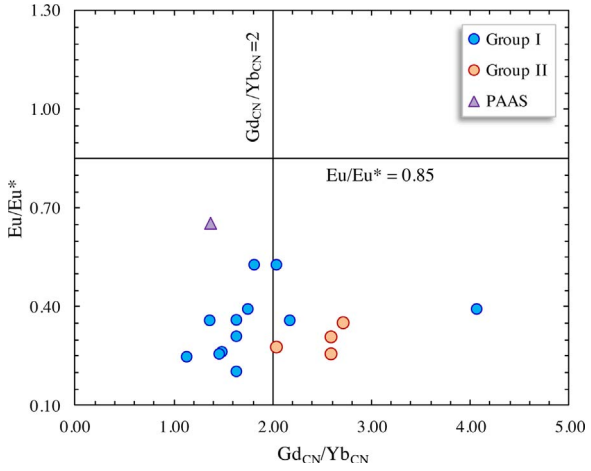

Fig. 8. Gd_{CN}/Yb_{CN} vs. Eu/Eu* plots for the Srisailam black shales. Note that the Group II shales mainly show > 2 Gd_{CN}/Yb_{CN} values. Such high ratios are characteristic of Archaean turbidites and sediments derived from Archaean Na-rich igneous rocks viz. tonalite, trondhjemite, and granodiorite (McLennan and Taylor, 1991). Note the greater magnitude of Eu-anomaly (< < 0.85) compared to the Archaean turbidites and sediments derived from the source rocks indicated above. Gd_{CN}/Yb_{CN} and Eu/Eu* values are after McLennan et al. (1990). Post-Archaean average Australian shale (PAAS; Taylor and McLennan, 1985) is also plotted for reference.

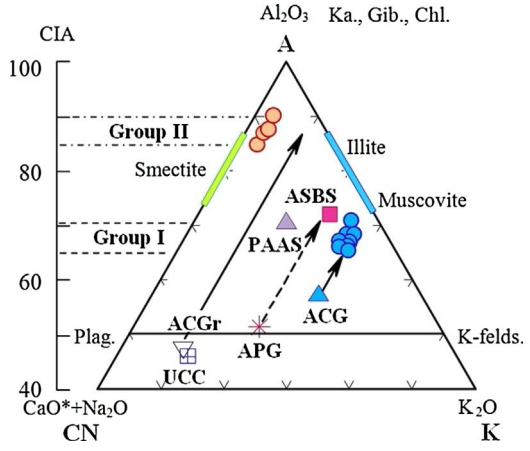

Fig. 9. A-CN-K compositional space (Nesbitt and Young, 1984) showing weathering trends for the Srisailam black shales. Solid arrows indicate idealized weathering trends from ACG for Group I shales, and from ACGr for Group II shales. Dotted arrow indicates weathering trend for APG as assumed source rock. Dashed and dash-dotted horizontal lines indicate ranges of CIA of Group I and II samples respectively. ASBS, average Srisailam black shale (this study); ACG, average Chitrial granite (unpublished data); ACGr, average Chitrial granodiorite (data from Vimal et al., 2012); APG, average Proterozoic granite (Condie, 1993); CIA, chemical index of alteration (Nesbitt and Young, 1982). UCC and PAAS data are from Taylor and McLennan (1985). Note the lack of any appreciable K-metasomatism (Fedo et al., 1995) in both the groups with respect to inferred source rocks. Also note the clustering of plots, which suggest steady-state of weathering (Nesbitt et al., 1997).

6.2. Palaeoweathering and palaeoclimate

The intensity of chemical weathering in the source area can be quantitatively evaluated using CIA (Nesbitt and Young, 1982). The CIA of the black shales as a whole shows wide range (65 − 90; Table 2). However, when considered group-wise, they show very restricted ranges, and cluster distinctly in A-CN-K plot (Fig. 9). The CIA of Group I samples (65–71, Av. 67 ± 2, n = 12) indicates moderate chemical weathering in the source area, while that of Group II samples (85–90, Av. 87 ± 2, n = 4) indicates more intense source area weathering. Additionally, such variation in CIA neither shows any correlation with Th/U ratio (Fig. 10a), nor anti-correlation with distance from the unconformity surface (Fig. 10b). It is evident that the sediments (Facies J or M; Fig. 2) deposited almost at the same time (assuming that at limited spatial separation, the relative time of deposition of the sediments is a linear function of its distance from the unconformity surface) show distinctly different CIA (Fig. 10b) implying varying degree of chemical weathering of the provenance at the same time. Since any particular provenance rock cannot undergo distinctly different degrees of chemical weathering at the same time, it is interpreted that such differences in CIA is due to variation in source rock composition. This interpretation is consistent with the inferred source rocks viz. granite and granodiorite for Group I and Group II shales respectively. Nesbitt and Young (1984) demonstrated that thermodynamic and kinetic stability of K^+ enables retention of K in weathered profile. Thus, preferential and more leaching of Ca and Na (Ca, Na > > K) will render higher CIA values for granodiorite or tonalite (containing more plagioclase) compared to granite (containing more K-feldspar) undergoing chemical weathering under the same climatic condition. The ICV values coupled with K_2O/Al_2O_3 ratios, indicating dominance of K-feldspar and plagioclase in Group I and Group II shales respectively, substantiate it.

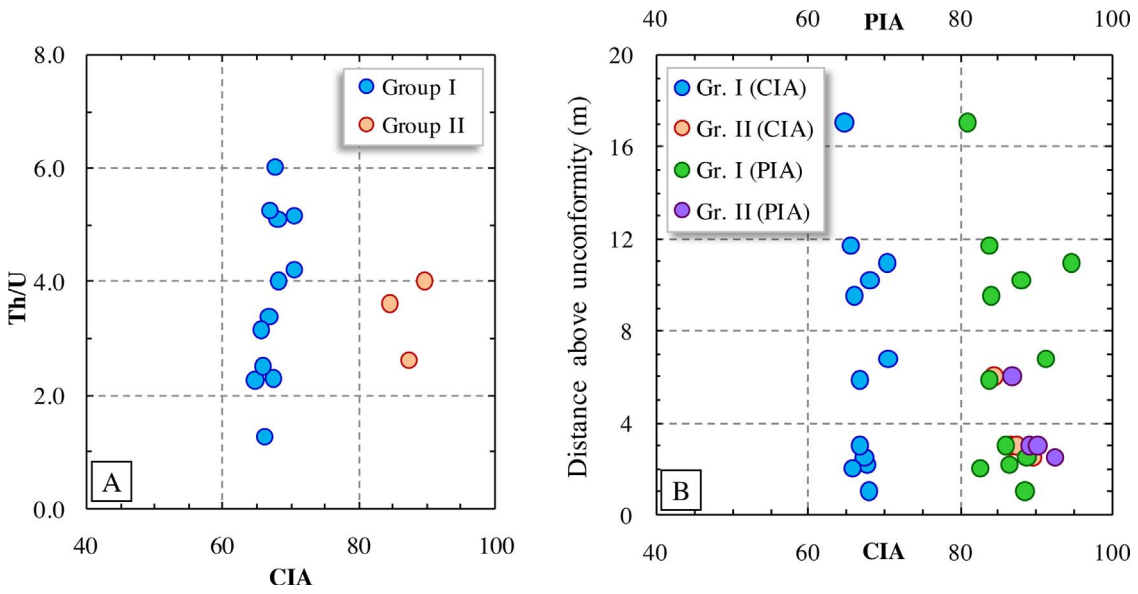

Fig. 10. (A) Plots of the Srisailam black shales in Th/U–CIA bivariate space. Note the lack of any correlation of CIA with Th/U ratio. This indicates that the variation of CIA of the Srisailam black shales is not related only to the intensity of chemical weathering of provenance rocks; (B) Plots of CIA vs. distances of the Srisailam black shale samples above the unconformity surface. Note the clustering of plots in two distinct groups and lack of any correlation of CIA values with distances from the unconformity surface. This indicates steady-state of weathering, and the variation in CIA is unrelated to the degree of chemical weathering. PIA, plagioclase index of alteration (Fedo et al., 1995).

Further, preferential leaching of these elements from the source granodiorite suite of rocks was additionally facilitated due to its hydrothermally altered (sericitized) nature (section 6.1). The non-correlation of Th/U with CIA also indicates that such variation in CIA is not related to variation in intensity of chemical weathering. However, before such conclusion it is also necessary to (i) monitor plagioclase weathering in both the source rock types, and (ii) examine signature of K enrichment in the shales due to K-metasomatism.

The overlapping PIA in black shales of both the groups (Fig. 10b) indicates near-uniform pattern of plagioclase weathering, and therefore similar intensity of chemical weathering. Slightly higher average PIA of Group II shales is due to hydrothermally alternated nature of their granodiorite (TGA; Vimal et al., 2012) source rock. The extent of K-metasomatism can be assessed by plotting the CIA values in A-CN-K compositional space (Fedo et al., 1995). Addition of potassium shifts the plots from the idealized weathering trend (parallel to the A-CN join; Fig. 9). We reasonably assume that the granites (ACG; Table 4), similar to those forming the basement for the Srisailam sediments and exposed in the vast terrane surrounding Chitrial outlier (Fig. 1c), were the source of Group I shales. Further, the tonalite-granodiorite-adamellite suite of rocks (ACGr; Table 4), occurring farther east and northeast of the study area (northeast of Peddavoora schist belt; Fig. 1c), were dominantly the source of Group II shales. The plots of CIA values in A-CN-K space follow the ideal weathering trends (Fig. 9), and thus nullify the possibility of any appreciable K-metasomatism of the sediments. Further, clustering of plots in A-CN-K space (Fig. 9) suggests steady-state of weathering (Nesbitt et al., 1997). Almost uniform CIA values in each group of samples irrespective of their distance from the unconformity surface (Fig. 10b) also indicate steady-state of weathering. Presumably, physical weathering was at par with or dominated over chemical weathering. Therefore, the differences in the CIA values are attributed to moderate chemical weathering of two compositionally different source rocks under semiarid climatic condition. In support it may be mentioned here that Biswas (2005) reported occurrence of aeolian sediments (marginal erg facies) and ephemeral fluvial deposits, characteristic of semiarid climate, from the southern parts of the Srisailam subbasin in and around the Krishna gorge (Fig. 1c). Moreover, the mid-latitude position of the Cuddapah basin (the Indian subcontinent) during 1450–1270 Ma (Pisarevsky et al., 2014) period also indicates semiarid palaeoclimatic condition during the deposition of the

Table 4
Average composition of the Srisailam black shales and their inferred source rocks.

	ACG (n = 99)	ACGr (n = 6)	Gr. I (n = 12)	Gr. II (n = 4)	ASBS (n = 16)	PAAS	APG	UCC
SiO_2	72.99 ± 2.24	65.86 ± 3.12	63.81 ± 6.08	63.48 ± 3.19	63.72 ± 5.40	62.80	73.30	66.00
TiO_2	0.25 ± 0.09	0.31 ± 0.10	0.35 ± 0.10	0.60 ± 0.06	0.41 ± 0.14	1.00	0.28	0.50
Al_2O_3	14.28 ± 1.53	16.35 ± 1.13	16.78 ± 2.39	17.83 ± 0.68	17.04 ± 2.12	18.90	13.50	15.20
Fe_2O_3(T)	2.30 ± 0.97	3.77 ± 1.42	4.45 ± 1.53	6.73 ± 1.28	5.02 ± 1.76	7.23	2.56	5.01
MnO	0.03 ± 0.03	0.04 ± 0.02	0.01	0.01	0.01	0.11	–	–
MgO	0.72 ± 0.51	1.39 ± 0.87	0.89 ± 0.25	1.18 ± 0.31	0.96 ± 0.29	2.20	0.42	2.20
CaO	0.27 ± 0.24	3.45 ± 1.60	0.18 ± 0.05	0.25 ± 0.06	0.20 ± 0.06	1.30	1.30	4.20
Na_2O	2.14 ± 0.92	5.25 ± 1.17	0.91 ± 0.20	0.98 ± 0.26	0.93 ± 0.21	1.20	3.20	3.90
K_2O	6.12 ± 1.10	3.13 ± 1.33	6.00 ± 0.76	0.63 ± 0.05	4.65 ± 2.49	3.70	4.80	3.40
P_2O_5	0.10 ± 0.09	0.15 ± 0.07	0.05 ± 0.03	0.03 ± 0.01	0.05 ± 0.03	0.16	0.08	–
K_2O/Na_2O	2.86 ± 1.46	0.67 ± 0.43	6.98 ± 2.18	0.69 ± 0.23	5.41 ± 3.38	3.08	1.50	0.87
K_2O/Al_2O_3	0.43 ± 0.07	0.19 ± 0.09	0.36 ± 0.01	0.035 ± 0.002	0.28 ± 0.15	0.20	0.36	0.22

ACG, average Chitrial granite (unpublished data); ACGr, average Chitrial granodiorite (average composition of TGA suite of rocks exposed east and northeast of Peddavoora schist belt; Vimal et al., 2012); ASBS, average Srisailam black shale (this study). Averages of two identified groups of black shales (Group I and II) are also given for comparison with respective source rocks. UCC (upper continental crust) and PAAS (post-Archaean average Australian shale) data are from Taylor and McLennan (1985). APG (average Proterozoic granite) data from Condie (1993).

Srisailam Formation.

6.3. Tectonic setting and basin evolution

The overall distribution of facies and their stacking pattern (Fig. 2) indicate that the sediments of the Srisailam Formation were deposited in continental half-graben basin(s), and the sediments in the study area represent deposits on the hanging-wall ramp. The presence of cohesionless debris flow (Facies A), hyperconcentrated flood flow (Facies B), and sheetflood deposits (Facies C) at the base of the sedimentary succession indicates deposition of initial sediments in dry alluvial fans (Bull 1977) along the basin margin. The presence of deep lacustrine sediments (Facies M) directly above the basement granite and above the sediments of alluvial fan/fan-delta facies association (FA-I) indicates development of lacustrine environment after the initial subsidence. The deep lacustrine sediments are overlain by sediments of delta front facies association (FA-III) related to progradation of delta into the lake water (Fig. 2). This indicates that the initial subsidence also led to enhancement of regional provenance gradient. The enhanced topographic gradient facilitated generation and supply of sediments at a greater rate than the subsidence rate of the basin floor (shallow water level) favouring delta progradation. Stacked repetition of delta channel sandstone (Facies E) of delta top facies association (FA-II; Fig. 2) indicates repeated incision and deposition of sediments in distributary channels. The presence of abundant randomly oriented platy grey shale fragments in Facies D (mouthbar) and Facies I (delta slope) also indicates incision of delta plain mudrocks. Such incision may be related to upheaval and increase in gradient due to rotation of the hanging-wall block during faulting (Leeder and Gawthorpe, 1987). The presence of near-shore (Facies F) and shallow water (Facies L) lacustrine facies sediments over the deltaic sediments indicates movement of pivot line up-dip of hanging-wall or regional peak subsidence (Fig. 2) of the basin floor, and transgression of lake water. Thus, this transgression event indicates regional extensional episode (Anderson et al., 1983; Leeder and Gawthorpe, 1987). Following peak subsidence a number of small parallel streams came into existence. Low sediment supply due to greater erosional maturity of the provenance coupled with partitioning of sediments into a number of streams, however, prevented fan development at this stage. The fluvial sediments were initially sufficiently reworked in the near-shore regions of the lake. However, later sediments of the fluvial facies association (FA-V) prograded inside the basin, possibly due to insufficient accommodation-space availability that resulted from pause in basin subsidence. A major flooding event at this stage possibly accentuated progradation of fluvial sediments inside the basin. The presence of thick wedges of Facies A or B directly over the basement granite well inside the basin indicates presence of intrabasinal fault-controlled uplifted basement segments.

The geochemical data of the black shales also provide equally significant insight into the tectonic setting and evolution of the Srisailam subbasin. K_2O/Na_2O–SiO_2 bivariate plot (Roser and Korsch, 1986) is widely used to discriminate tectonic setting of deposition of siliciclastic rocks. However, enhancement of K_2O/Na_2O ratio, due to diagenetic loss of Na and/or addition of K independently or in a combined way, is a constraint to use of this plot. Additionally, enhanced influence or proximity of mafic source rocks especially continental flood basalts, thereby lowering K_2O/Na_2O ratio, may be another constraint (Saha et al., 2010). Only marginal increase in K_2O/Na_2O ratio compared to their inferred source rocks (Table 4), and lack of any geochemical signature of significant K addition in both Group I and II shales allow the use of K_2O/Na_2O–SiO_2 bivariate plot. Similarly, the REE patterns of the studied shales rule out enhanced influence or proximity of mafic source rocks. In K_2O/Na_2O–SiO_2 bivariate space majority of the black shale samples plot in the 'passive margin' field (Fig. 11). Under such a tectonic set-up sediments are derived from stable continental areas and deposited in plate interiors or intracratonic basins (Roser and Korsch, 1986), Atlantic-type rifted continental margin basins, and intracratonic rift-bounded grabens (Bhatia, 1983; Roser and Korsch, 1986). Four samples falling in the 'active continental margin' field indicate derivation of the sediments from 'uplifted basement' (see Roser and Korsch, 1986) that flanked intrabasinal faults. Interestingly all the four samples belong to Group II shales. This implies that their inferred 'granodiorite' source rocks possibly formed major part of the uplifted basement segments. As the sediments, derived from these uplifted basement segments, were transported for a limited distance before deposition their K_2O/Na_2O ratios were only marginally enhanced compared to their source rocks (Table 4). The presence of uplifted basement segment well inside the basin is characteristic of many continental (intracratonic) half-graben basins. Therefore, it is inferred that the deposition of the Srisailam shales took place in continental rift basin.

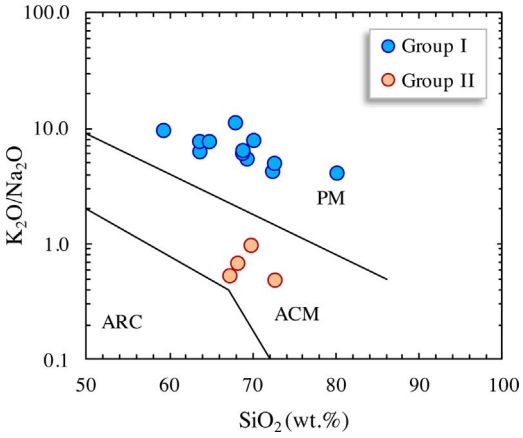

Fig. 11. K_2O/Na_2O vs.SiO_2 tectonic setting discrimination plot for the Srisailam black shales. Field boundaries are after Roser and Korsch (1986). PM, passive margin [basins on continental crust, and basins associated with ocean floor spreading, failed rifts and Atlantic-type continental margins]; ACM, active continental margin [continental margin magmatic arcs (including trench, forearc, intraarc, and backarc basins), continental collision basins, and pull-apart basins associated with strike-slip fault zones]; ARC, oceanic island arc margin [oceanic island arc (including forearc, intraarc, and backarc basins and trenches)].

An idea about the tectonic setting can also be obtained from chondrite-normalized REE data. According to McLennan (1989), LREE enrichment, flat HREE pattern, the ubiquitous negative Eu-anomaly, and the overall REE pattern fairly uniform and similar to PAAS are characteristics of sediments deposited at passive margins. The chondrite-normalized REE patterns (Fig. 5a and b) of the Srisailam black shales are fairly uniform and similar to PAAS, and therefore indicate passive margin setting for their deposition. Average La_{CN}/Yb_{CN}, La_{CN}/Sm_{CN} ratios and Eu-anomalies of the Srisailam shales are typical of passive margin muds. La/Sc, La/Y, and Ce/Sc ratios also reveal passive margin depositional setting (Table 5). Sediments deposited in active margin set up are characterized by low Th/Sc (< 0.01–1.80) ratio (McLennan et al., 1990). High Th/Sc ratios of the Srisailam black shales

Table 5
Averages of depositional setting indicator some critical trace elemental ratios in the Srisailam black shales.

Ratio	Group I	Group II	TE†	CA†	FA†
La_{CN}/Yb_{CN}	11.77	10.37	10.02	6.25	3.41
La_{CN}/Sm_{CN}	2.99	3.92	3.61	2.75	2.06
Eu/Eu*	0.35	0.30	0.68	0.74	0.88
La/Sc	2.5	17.0	3.6	1.7	0.6
La/Y	1.8	1.6	1.3	1.0	0.5
Ce/Sc	4.8	33.5	7.3	3.2	1.1
Th/Sc	2.66	8.50	2.46	0.59	0.11

†Averages of the same ratios from modern trailing edge (passive margin, TE), continental arc (CA) and forearc (FA) muds are also presented for comparison (data from McLennan et al., 1990).

(Table 5) also indicate passive margin depositional setting.

6.4. Timing of Columbia breakup

During the Proterozoic eon all or nearly all of the continental blocks were amalgamated at least twice resulting in the formation of two supercontinents − Columbia (ca. 1800–1500 Ma) and Rodinia (ca. 1100–700 Ma; Rogers and Santosh, 2002). The intervening period witnessed the rifting of Columbia and its reassembly to form younger supercontinent Rodinia. However, the exact timing of breakup of Columbia has been debated long. Rogers and Santosh (2002) suggested that the fragmentation of Columbia occurred from ~1.6 Ga to 1.4 Ga. The widespread Mesoproterozoic continental rifting and emplacement of abundant ca. 1.6–1.3 Ga anorogenic magmatism in most cratonic blocks worldwide have been considered to be associated with the breakup of Columbia. A dismembered granite-rhyolite terrane in the Mahanadi and the Godavari rifts (initiated at ~1.5 Ga), and the Dalma mafic/ultramafic rocks (~1.6 Ga) from India have been shown as the evidence of fragmentation of Columbia (Rogers and Santosh, 2002). Further, the ca. 1500–1400 Ma sub-alkaline basalts in the Eastern Ghats, and mantle plume induced ca. 1400 Ma lamproite and kimberlite magmatism in the Cuddapah basin (Fig. 1a) have been correlated with extensional phases associated with the breakup of Columbia (Chakraborty et al., 2010; Chalapathi Rao et al., 2014). Contrary to this, gravity modeling and seismic studies on Eastern Ghat Mobile Belt (Mishra and Kumar, 2014) suggest crustal thickening and E-W convergence during 1.5–1.0 Ga. Globally, the emplacement of the 1.27 Ga Mackenzie and 1.24 Ga Sudbury mafic dike swarms has been shown to mark the final breakup of the supercontinent at about 1.3–1.2 Ga (Zhao et al., 2004). However, Shellnutt and MacRae (2012) have recently shown that the Sudbury dyke swarms in Laurentia are unrelated to a mantle plume or the break-up of a supercontinent. Yakubchuk (2010) on the basis of kinematic and palaeomagnetic reconstruction of 645 individual terranes worldwide suggested that Columbia was amalgamated by ca. 1.85 Ga and remained largely intact until 1.1–1.0 Ga. According to Pesonen et al. (2012) the amalgamation of Columbia did not happen until ca. 1.53 Ga, and it broke up at ca. 1.18 Ga during several rifting episodes.

Juvenile curst production and regional- to global-scale magmatic events, viz. emplacement of giant dyke swarms, extrusion of flood basalts, anorogenic magmatism, are natural proxies for supercontinent breakup/formation and mantle superplume events. Moreover, BIFs and especially black shales have been shown to proxy for supercontinent breakup/formation and mantle superplume events (Condie et al., 2001; Condie, 2004). Enhanced deposition of black shales correlates with superplume events and with supercontinent breakup (Condie, 2004). During breakup of supercontinents, new ocean-ridges form and the input of CO_2 into the atmosphere–ocean system increases (Condie, 2004). Increasing atmospheric CO_2 levels and rising sea level promote warmer climates that in turn increase weathering rates (Berner and Berner, 1997). The important effects of supercontinent breakup are marine transgression and increased rate of burial of organic and carbonate carbon on stable continental shelves, increase in the $\delta^{13}C$ of seawater reciprocal to the deposition of organic carbon, and higher CIA values of the black shales (Condie et al., 2001). Similarly, during a superplume event input of both CO_2 and reduced constituents into the ocean–atmosphere system is enhanced due to plume volcanism and associated hydrothermal activity (Condie et al., 2001). The increased CO_2 flux warms the climate and enhances weathering rates (Berner and Berner, 1997). Phenomena associated with superplume events viz. enhanced influx of CO_2, weathering of landmasses, marine transgression, hydrothermal activity on the sea floor, carbonate precipitation, biological productivity, and organic matter burial etc. promote the formation and deposition of both organic and carbonate carbon (Condie et al., 2001). In contrast, supercontinent formation promotes higher rates of erosion and sedimentation, marine regression, restricted deposition of platformal carbonate, high ratios of organic versus carbonate carbon sedimentation, and positive $\delta^{13}C$ in seawater (Condie et al., 2001). During supercontinent formation, organic carbon sedimentation occurs either farther offshore or in freshwater depocenters within the interior of the supercontinent (Berner, 1983).

The sedimentological as well as geochemical data have revealed that the Srisailam Formation was deposited in half-graben-like intracratonic depression well inside the Eastern Dharwar Craton. Further, the Srisailam Formation is notably devoid of carbonates, and is characterized by high 'black shale' to 'total shale' ratio (> 0.51) and restricted thickness (up to 29.0 m) of black shale. In the light of the discussion in the preceding paragraph, it may be inferred that the deposition of the Srisailam sediments took place during a period while supercontinent assembly was continuing i.e., the Palaeo-Mesoproterozoic supercontinent Columbia was still growing on. During supercontinent formation increased extraction of CO_2 from atmosphere on account of weathering of growing landmass produces global cooling. This is reflected in lower CIA values of black shales and other terrigenous sediments deposited during the formation of supercontinents. The CIA values (65–90, Av. 73 ± 10) of the Srisailam black shales reflect overall moderate chemical weathering. Moreover, the observed low in black shale abundance and CIA is in agreement with global lows around 1350 Ma (Fig. 2 in Condie et al., 2001). Slightly higher average CIA value of the Srisailam black shales (due to relatively higher plagioclase weathering) may be positive feedback (hydrothermal alteration) of isolated mantle event(s) prior to the initiation of the Srisailam subbasin, when a number of plumes rose and impinged at the base of the lithosphere of the region. Such plume events were possibly unrelated to any global mantle upwelling or fragmentation process of Columbia. It may be mentioned here that geodynamic modeling for the genesis of the lamproites of the Cuddapah basin (Fig. 1a) has also indicated only small amounts of lithospheric extension (Chalapathi Rao et al., 2004) in the region. To summarise, global rise in sea level, atmospheric CO_2, and climatic temperature related to large-scale breakup of the supercontinent Columbia did not take place during the interval of deposition (1400–1327 Ma) of the Srisailam sediments. Supporting evidence also comes from the recent studies that indicate continued growth of Columbia by external accretion throughout the Mesoproterozoic, and its breakup during a pan-global rifting event at ~1.2 Ga (Zhao et al., 2004; Yakubchuk, 2010; Pesonen et al., 2012). Further large-scale rifting and breakup of supercontinent would ultimately lead to shallow marine sedimentation on the flanks of passive margin. Global lower abundance of passive margins (Bradley, 2008) during the Mesoproterozoic (until 1.25 Ga) also indicates that large scale break-up of Columbia did not take place until 1.25 Ga (Roberts, 2013).

7. Conclusions

- Preliminary sedimentological studies and analysis of sedimentary facies of the Srisailam Formation in Chitrial outlier indicates deposition of the Srisailam Formation in continental half-graben basin (s). The studied black shales (*sensu lato*) were deposited in deep lacustrine and prodelta facies.
- The Srisailam black shales are enriched in K_2O, Rb, Cr, Th, U, and Pb, and depleted in CaO, Na_2O, TiO_2, Al_2O_3, P_2O_5, Sr, Ba, Y, Zr, Sc, V, Ni, Cu, and Zn compared to PAAS at similar SiO_2 contents. The shales show moderately fractionated LREE (Av. La_{CN}/Sm_{CN}, 3.23 ± 0.87) and relatively flat HREE (Av. Gd_{CN}/Yb_{CN}, 1.99 ± 0.72) characteristics with chondrite-normalized REE patterns broadly similar to that of PAAS.
- TiO_2/Zr and Al_2O_3/TiO_2 ratios coupled with provenance indicator critical trace elemental ratios viz. La/Sc, Th/Sc, Th/Cr, and Eu/Eu* indicate derivation of the shales from cratonic felsic igneous source rocks. Al_2O_3–TiO_2 bivariate plot and Gd_{CN}/Yb_{CN} values (1.12–4.05, Av. 1.99 ± 0.72) indicate heterogeneity of the provenance, and presence of at least two types of source rock – granite and

granodiorite. The overlapping Al_2O_3/TiO_2 ratio and REE signatures indicate limited mixing of the sediments from these sources also.

- The K_2O contents, K_2O/Na_2O and K_2O/Al_2O_3 ratios, CIA, and ICV values of the Srisailam shales show bimodality. The plots of the samples in A-CN-K compositional space do not show any evidence of K-metasomatism. On the basis of comparable PIA, lack of geochemical signature of diagenetic K addition, and non-correlation of CIA with Th/U ratio, the observed differences in CIA are interpreted in terms of heterogeneity in source rock composition. The plots of the samples in A-CN-K diagram also indicate steady-state weathering of the source rock(s) under semiarid climate.
- Sedimentary facies and geochemical characteristics of the Srisailam Formation indicate continental rift basin (passive margin) depositional setting. Stable tectonic setting and semiarid climatic condition favoured steady-state weathering and erosion of highly differentiated upper crustal continental provenances.
- Geochemical and sedimentological characteristics of the Srisailam black shales do not reflect any global rise in sea level, atmospheric CO_2, and climatic temperature related to supercontinent breakup, and thereby largely exclude any large-scale breakup of the Palaeo-Mesoproterozoic supercontinent Columbia during the interval (1400–1327 Ma) of deposition of the Srisailam Formation.

Acknowledgements

The authors are thankful to Prof. Alexander Deutsch for encouraging editorial handling. The valuable suggestions and comments by two anonymous reviewers have helped immensely to improve the presentation of the manuscript. The authors are indebted to them. The authors are grateful to the Director, AMD for giving permission to publish this work. Thanks are due to Dr. Rahul Banerjee for critically reviewing the manuscript under the purview of departmental review process. The authors are also thankful to Dr. K. Krishnakumar and other officers of the Chemical Laboratory, AMD, Hyderabad for providing analytical support.

Appendix A. Supplementary data

Supplementary data associated with this article can be found, in the online version, at http://dx.doi.org/10.1016/j.chemer.2017.10.002.

References

Anderson, R.E., Zoback, M.L., Thompson, G.A., 1983. Implications of selected subsurface data on the structural form and evolution of some basins in the northern Basin and Range Province, Nevada and Utah. Bull. Geol. Soc. Am. 94, 1055–1072.
Banerjee, S., Dutta, S., Paikaray, S., Mann, U., 2006. Stratigraphy, sedimentology and bulk organic geochemistry of black shales from the Proterozoic Vindhyan Supergroup (central India). J. Earth Syst. Sci. 115, 37–47.
Banerjee, R., Bahukhandi, N.K., Rahman, M., Achar, K.K., Ramesh Babu, P.V., Umamaheswar, K., Parihar, P.S., 2012. Lithostratigraphic and radiometric appraisal of deeper parts of Srisailam and Palnad sub-basins in Kottapullareddipuram-Achchammagunta-Rachchamallepadu area, Guntur district, Andhra Pradesh. Expl. Res. At. Miner. 22, 55–69.
Basu, H., Kumar, K.M., Paneerselvam, S., Chaki, A., 2009. Study of provenance characteristics and depositional history on the basis of U, Th and K abundances in the Gulcheru Formation, Cuddapah Basin in Tummalapalle-Somalollapalle areas, Cuddapah-Anantapur districts, Andhra Pradesh. J. Geol. Soc. India 74, 318–328.
Basu, H., Sastry, R.S., Achar, K.K., Umamaheswar, K., Parihar, P.S., 2014. Palaeoproterozoic fluvio-aeolian deposits from the lower Gulcheru Formation Cuddapah Basin, India. Precambrian Res. 246, 321–333.
Berner, R.A., Berner, E.K., 1997. Silicate weathering and climate. In: Ruddiman, W.F. (Ed.), Tectonic Uplift and Climate Change. Plenum Press, New York.
Berner, R.A., 1983. Burial of organic carbon and pyrite sulphur in sediments over Phanerozoic time: a new theory. Geochim. Cosmochim. Acta 47, 855–862.
Bhatia, M.R., 1983. Plate tectonics and geochemical composition of sandstones. J. Geol. 91, 611–627.
Biswas, A., 2005. Coarse aeolianites: sand sheets and zibar-interzibar facies from the Mesoproterozoic Cuddapah Basin, India. Sediment. Geol. 174, 149–160.
Bradley, D.C., 2008. Passive margins through earth history. Earth Sci. Rev. 91, 1–26.
Bull, W.B., 1977. The alluvial-fan environment. Prog. Phys. Geogr. 1, 222–270.
Chakraborty, P.P., Dey, S., Mohanty, S.P., 2010. Proterozoic platform sequences in Peninsular India: Implications towards basin evolution and supercontinent assembly. J. Asian Earth Sci. 39, 589–607.
Chalapathi Rao, N.V., Miller, J.A., Gibson, S.A., Pyle, D.M., Madhavan, V., 1999. Precise $^{40}Ar/^{39}Ar$ dating of Kotakonda kimberlite and Chelima lamproite, India: Implication to the timing of mafic dyke swarm activity in the Eastern Dharwar craton. J. Geol. Soc. India 53, 425–432.
Chalapathi Rao, N.V., Gibson, S.A., Pyle, D.M., Dickin, A.P., 2004. Petrogenesis of Proterozoic lamproites and kimberlites from the Cuddapah basin and Dharwar cratons, southern India. J. Petrol. 45, 907–948.
Chalapathi Rao, N.V., Kumar, A., Sahoo, S., Dongre, A.N., Talukdar, D., 2014. Petrology and petrogenesis of Mesoproterozoic lamproites from the Ramadugu field, NW margin of the Cuddapah basin, Eastern Dharwar craton, southern India. Lithos 196–197, 150–168.
Chatterjee, N., Bhattacharji, S., 2001. Petrology, geochemistry and tectonic settings of the mafic dikes and sills associated with the evolution of the Proterozoic Cuddapah Basin of south India. Proc. Indian Acad. Sci. (Earth Planet. Sci.) 110, 433–453.
Collins, A.S., Patranabis-Deb, S., Alexander, E., Bertram, C.N., Falster, G.M., Gore, R.J., Mackintosh, J., Dhang, P.C., Saha, D., Payne, J.L., Jourdan, F., Backé, G., Halverson, G.V., Wade, B.P., 2015. Detrital mineral age, radiogenic isotopic stratigraphy and tectonic significance of the Cuddapah Basin, India. Gondwana Res. 28, 1294–1309. http://dx.doi.org/10.1016/j.gr.2014.10.013.
Condie, K.C., Des Marais, D.J., Abbott, D., 2001. Precambrian superplumes and supercontinents: a record in black shales, carbon isotopes, and paleoclimates. Precambrian Res. 106, 239–260.
Condie, K.C., 1993. Chemical composition and evolution of the Upper continental crust: contrasting results from surface samples and shales. Chem. Geol. 104, 1–37.
Condie, K.C., 2004. Supercontinents and superplume events: distinguishing signals in the geologic record. Phys. Earth Planet. Inter. 146, 319–332.
Cox, R., Lowe, D.R., 1995. Controls on sediment composition on a regional scale: a conceptual review. J. Sediment. Res. A 5, 1–12.
Cox, R., Lowe, D.R., Cullers, R.L., 1995. The influence of sediment recycling and basement composition on evolution of mudrock chemistry in the southwestern United States. Geochim. Cosmochim. Acta 59, 2919–2940.
Crawford, A.R., Compston, W., 1973. The age of the Cuddapah and Kurnool systems, southern India. J. Geol. Soc. Aust. 19, 453–464.
Cullers, R.L., Podkovyrov, V.N., 2000. Geochemistry of the Mesoproterozoic Lakhanda shales in southeastern Yakutia, Russia: implications for mineralogical and provenance control, and recycling. Precambrian Res. 104, 77–93.
Cullers, R.L., 2000. The geochemistry of shales, siltstones and sandstones of Pennsylvanian-Permian age, Colorado, USA: Implications for provenance and metamorphic studies. Lithos 51, 181–203.
Dasgupta, P., 2003. Sediment gravity flow – the conceptual problems. Earth Sci. Rev. 62, 265–281.
Dutt, N.V.B.S., 1975. Geology and Mineral Resources of Andhra Pradesh. Ramesh Publications, Hyderabad 205p.
Esmaeili, D., Afshouni, S.Z., 2009. The study of mass changes during hydrothermal alteration in the Astaneh granitoid (SW of Arak). Geosciences 18, 97–104.
Fedo, C.M., Nesbitt, H.W., Young, G.M., 1995. Unraveling the effects of potassium metasomatism in sedimentary rocks and paleosols, with implications for paleoweathering conditions and provenance. Geology 23, 921–924.
Fralick, P.W., 2003. Geochemistry of clastic sedimentary rocks: ratio techniques. In: Lenz, D.R. (Ed.), Geochemistry of Sediments and Sedimentary Rocks: Evolutionary Considerations to Mineral Deposit-Forming Environments. Geological Association of Canada GeoText 4, pp. 85–103.
French, J.E., Heaman, L.M., Chacko, T., Srivastava, R.K., 2008. 1891–1883 Ma Southern Bastar–Cuddapah mafic igneous events, India: a newly recognized Large Igneous Province. Precambrian Res. 160, 308–322.
Hayashi, K., Fujisawa, H., Holland, H.D., Ohmoto, H., 1997. Geochemistry of ~1.9 Ga sedimentary rocks from northeastern Labrador, Canada. Geochim. Cosmochim. Acta 61, 4115–4137.
King, W., 1872. On the Kadapah and Kurnúl Formations in the Madras Presidency. Memoir of the Geological Survey of India. pp. 8.
Krishnaswamy, V.S., Murty, Y.G.K., Nagaraja Rao, B.K., Ramalyngaswamy, G., Rajurkar, S.T., Mehdi, S.H., Setti, D.N., Madan Mohan, B., Ravindra Babu, B., 1981. Geological and Mineral Map of Cuddapah Basin. Geological Survey of India, Hyderabad.
Lakshminarayana, G., Bhattacharjee, S., Ramanaidu, K.V., 2001. Sedimentation and stratigraphic framework in the Cuddapah Basin. Geol. Surv. India Special Publ. 55, 31–58.
Leeder, M.R., Gawthorpe, R.L., 1987. Sedimentary models for extensional tilt-block/half-graben basins. In: Coward, M.P., Dewey, J.F., Hancock, P.L. (Eds.), Continental Extensional Tectonics. Geological Society London, pp. 139–152 (Special Publication 28).
Manikyamba, C., Kerrich, R., 2006. Geochemistry of Black shales from the Neoarchean Sandur Superterrane, India: first cycle volcanogenic sedimentary rocks in an intraoceanic arc-trench complex. Geochim. Cosmochim. Acta 70, 4663–4679.
Manikyamba, C., Kerrich, R., González-Álvarez, I., Mathur, R., Khanna, T.C., 2008. Geochemistry of Paleoproterozoic black shales from the Intracontinental Cuddapah basin, India: implications for provenance, tectonic setting, and weathering intensity. Precambrian Res. 162, 424–440.
McLennan, S.M., Taylor, S.R., 1991. Sedimentary rocks and crustal evolution: tectonic setting and secular trends. J. Geol. 99, 1–21.
McLennan, S.M., Fryer, B.J., Young, G.M., 1979. The geochemistry of the carbonate-rich Espanola Formation (Huronian) with emphasis on the rare earth elements. Can. J. Earth Sci. 16, 230–239.
McLennan, S.M., Taylor, S.R., McCulloch, M.T., Maynard, J.B., 1990. Geochemical and Nd-Sr isotopic composition of deep-sea turbidites: Crustal evolution and plate

tectonic associations. Geochim. Cosmochim. Acta 54, 2015–2050.
McLennan, S.M., Bock, B., Hemming, R., Hurowitz, J.A., Lev, S.M., McDaniel, D.K., 2003. The roles of provenance and sedimentary processes in the geochemistry of sedimentary rocks. In: Lenz, D.R. (Ed.), Geochemistry of Sediments and Sedimentary Rocks: Evolutionary Considerations to Mineral Deposit-Forming Environments. Geological Association of Canada, GeoText 4, pp. 7–31.
McLennan, S.M., 1989. Rare earth elements in sedimentary rocks: influence of provenance and sedimentary processes. In: In: Lipin, B.R., McKay, G.A. (Eds.), Geochemistry and Mineralogy of REE. Reviews in Mineralogy, vol. 2. pp. 169–200.
Meijerink, A.M.J., Rao, D.P., Rupke, J., 1984. Stratigraphic and structural development of the Precambrian Cuddapah basin, S.E. India. Precambrian Res. 26, 57–104.
Mishra, D.C., Kumar, M. Ravi, 2014. Proterozoic orogenic belts and rifting of Indian cratons: geophysical constraints. Geosci. Front. 5, 25–41.
Murthy, Y.G.K., 1979. Salient features of the revised geological map of the Cuddapah basin. In: 3rd Workshop on Status, Problems and Programmes in Indian Peninsular Shield. Institute of Indian Peninsular Geology, Hyderabad,. pp. 1–21.
Murty, P.S.N., Aswathanarayana, U., Mahadevan, C., 1962. Geochemistry of the siliceous black shales at Nagarjunasagar damsite, India. Econ. Geol. 57, 614–616.
Nagaraja Rao, B.K., Rajurkar, S.T., Ramalingaswamy, G., Ravindra Babu, B., 1987. Stratigraphy, structure and evolution of the Cuddapah Basin. In: In: Radhakrishna, B.P. (Ed.), Purana Basins of Peninsular India (Middle to Late Proterozoic), vol. 6. The Geological Society of India Memoire, pp. 33–86.
Nesbitt, H.W., Young, G.M., 1982. Early Proterozoic climates and plate motions inferred from major element chemistry of lutites. Nature 299, 715–717.
Nesbitt, H.W., Young, G.M., 1984. Prediction of some weathering trends of plutonic and volcanic rocks based on thermodynamic and kinetic considerations. Geochim. Cosmochim. Acta 48, 1523–1534.
Nesbitt, H.W., Fedo, C.M., Young, G.M., 1997. Quartz and feldspar stability, steady and non-steady-state weathering and pedogenesis of siliciclastics sands and muds. J. Geol. 105, 173–191.
Paikaray, S., Banerjee, S., Mukherji, S., 2008. Geochemistry of shales from the Paleoproterozoic to Neoproterozoic Vindhyan Supergroup: Implications on provenance, tectonics and paleoweathering. J. Asian Earth Sci. 32, 34–48.
Pandalai, H.S., Majumder, T., Chandra, D., 1983. Geochemistry of pyrite and black shales of Amjhore Rohtas District, Bihar, India. Econ. Geol. 78, 1505–1513.
Pandey, B.K., Gupta, J.N., Sarma, K.J., Sastry, C.A., 1997. Sm-Nd, Pb–Pb and Rb-Sr geochronology and petrogenesis of the mafic dyke swarm of Mahbubnagar, South India: implications for Paleoproterozoic crustal evolution of the Eastern Dharwar Craton. Precambrian Res. 84, 181–196.
Pandey, B.K., Veenakrishna, Pandey, U.K., Sastry, D.V.L.N., 2009. Radiometric dating of uranium mineralization in the Proterozoic basins of eastern Dharwar craton, south India. Peaceful uses of Atomic Energy 2009, 116–117.
Parihar, P.S., Rao, J.S., 2012. Cuddapah basin − a uranium province. Expl. Res. At. Miner. 22, 1–19.
Parsapoor, A., Dilles, J.H., Khalili, M., 2015. Discrimination between mineralized and unmineralized alteration zones by using surficial geochemical and primary hallows of the Darreh -Zar porphyry Cu -Mo deposit, Southeast of Iran. Goldschmidt 2414 (Abstracts).
Pesonen, L.J., Mertanen, S., Veikkolainen, T., 2012. Palaeo-Mesoproterozoic supercontinents −A paleomagnetic view. Geophysica 48, 5–47.
Pisarevsky, S.A., Elming, S-Å., Pesonen, L.J., Li, Z.-X., 2014. Mesoproterozoic paleogeography: Supercontinent and beyond. Precambrian Res. 244, 207–225.
Pradhan, V.R., Meert, J.G., Pandit, M.K., Kamenov, G., Gregory, L.C., Malone, S.J., 2009. India's changing place in global Proterozoic reconstructions: a review of geochronologic constraints and paleomagnetic poles from the Dharwar, Bundelkhand and Marwar cratons. J. Geodyn. 50, 224–242. http://dx.doi.org/10.1016/j.jog.2009.11.008.
Rajurkar, S.T., Ramalingaswami, G., 1975. Facies variation within the upper Cuddapah strata in the northern part of Cuddapah basin. Geol. Surv. India Misc. Publ. 23, 150–157.
Rawat, T.P.S., Joshi, G.B., Basu, B., Absar, N., 2010. Occurrence of Proterozoic black shale-hosted uranium mineralisation in Tal Group, Sirmour District, Himachal Pradesh. J. Geol. Soc. India 75, 709–714.
Roberts, N.M.W., 2013. The boring billion?-Lid tectonics, continental growth and environmental change associated with the Columbia supercontinent. Geosci. Front. 4, 681–691.
Rogers, J.W.J., Santosh, M., 2002. Configuration of Columbia, a Mesoproterozoic Supercontinent. Gondwana Res. 5, 5–22.
Roser, B.P., Korsch, R.J., 1986. Determination of tectonic setting of sandstone-mudstone suites using SiO_2 content and K_2O/Na_2O ratio. J. Geol. 94, 635–650.
Saha, S., Banerjee, S., Burley, S.D., Ghosh, A., Saraswati, P.K., 2010. The influence of flood basaltic source terrains on the efficiency of tectonic setting discrimination diagrams: An example from the Gulf of Khambhat, western India. Sed. Geol. 228, 1–13.
Saha, D., 2002. Multi-stage deformation in the Nallamalai fold belt, Cuddapah basin, South India −Implications for Mesoproterozoic tectonism along southeastern margin of India. Gondwana Res. 5, 701–719.
Schieber, J., 1992. A combined petrographical-geochemical provenance study of the Newland formation, Mid-Proterozoic of Montana. Geol. Mag. 129, 223–237.
Shellnutt, J.G., MacRae, N.D., 2012. Petrogenesis of the Mesoproterozoic (1.23 Ga) Sudbury dyke swarm and its questionable relationship to plate separation. Int. J. Earth Sci. 101, 3–23.
Swanson, V.E., 1961. Geology and Geochemistry of Uranium in Marine Black Shales − A Review. U.S. Geological Survey, Professional Paper 356-C. United States Government Printing Office, Washington 112 pp.
Taylor, S.R., McLennan, S.M., 1985. The Continental Crust: Its Composition and Evolution. Blackwell Scientific Publications, Oxford, pp. 312p.
Taylor, S.R., McLennan, S.M., McCulloch, M.T., 1983. Geochemistry of loess, continental crustal composition and crustal model ages. Geochim. Cosmochim. Acta 47, 1897–1905.
Tourtelot, H.A., 1979. Black shale − its deposition and diagenesis. Clays and Clay Minerals 27, 313–321.
Vimal, R., Banerjee, R., Gupta, S., Veenakrishna, Achar, K.K., Ramesh Babu, P.V., Parihar, P.S., Maithani, P.B., 2012. Geochemistry and Sr and Pb isotope systematic of basement granitoids from North and West of Palnad sub-basin, Guntur and Nalgonda districts, Andhra Pradesh. J. Appl. Geochem. 14, 295–315.
Williams, J.C., Basu, A.R., Bhargava, O.N., Ahluwalia, A.D., Hannigan, R.E., 2012. Resolving original signatures from a sea of overprint −The geochemistry of the Gungri Shale (Upper Permian, Spiti Valley, India). Chem. Geol. 324–325, 59–72.
Yakubchuk, A., 2010. Restoring the supercontinent Columbia and tracing its fragments after its breakup: A new configuration and a Super-Horde hypothesis. J. Geodyn. 50, 166–175.
Zhao, G., Sun, M., Wilde, S.A., Li, S., 2004. A Palaeo-Mesoproterozoic supercontinent: assembly, growth and breakup. Earth Sci. Rev. 67, 91–123.